The Requirement of Ubiquitin C-Terminal Hydrolase L1 (UCHL1) in Mouse Ovarian Development and Fertility

Morgan F. Woodman[1], Meghan C.H. Ozcan[2,3], Megan A. Gura[4], Payton De La Cruz[1,5], Alexis K. Gadson[2,3], , Kathryn J. Grive[1,2]

[1] Women and Infants Hospital of Rhode Island, Department of Obstetrics and Gynecology, Program in Women's Oncology, Providence, RI 02905
[2] Women and Infants Hospital of Rhode Island, Department of Obstetrics and Gynecology, Reproductive Endocrinology and Infertility Fellowship Program, Providence, RI 02905
[3] Warren Alpert Medical School of Brown University, Department of Obstetrics and Gynecology, Providence, RI 02905
[4] Brown University, MCB Graduate Program and Department of Molecular Biology, Cell Biology, and Biochemistry, Providence, RI, 02906
[5] Brown University, Pathobiology Graduate Program, Providence, RI, 02906

Corresponding author: EMAIL kgrive@wihri.org; PHONE (401)-274-1122 ext: 48031;
Kilguss Research Institute, 200 Chestnut St., Room 108, Providence, RI 02903, USA

Grant support: This work was supported in part by the NIH P20 GM121298 (COBRE for Reproductive Health) grant as well as funding from Swim Across America.

Running title: UCHL1 in Mouse Ovarian Development and Fertility

Summary sentence: Ubiquitin C-Terminal Hydrolase L1 (UCHL1) is required for proper ovarian folliculogenesis, estrus cyclicity, and fertility in the female mouse.

Keywords: ovary, ovarian reserve, oocyte, ubiquitin, endocrine, estrus, ovulation

ABSTRACT:

Ubiquitin C-Terminal Hydrolase L1 (UCHL1) is a de-ubiquitinating enzyme enriched in neuronal and gonadal tissues known to regulate the cellular stores of mono-ubiquitin and protein turnover. While its function in maintaining proper motor neuron function is well-established, investigation into its role in the health and function of reproductive processes is only just beginning to be studied. Single-cell-sequencing analysis of all ovarian cells from the murine perinatal period revealed that *Uchl1* is very highly expressed in the developing oocyte population, an observation which was corroborated by high levels of oocyte-specific UCHL1 protein expression in oocytes of all stages throughout the mouse reproductive lifespan. Interestingly, expression of *Uchl1* is highly correlated with other master regulators of oocyte development, *Figla*, *Sohlh1*, and *Lhx8*. To better understand the role UCHL1 may be playing in oocytes, we utilized a UCHL1-deficient mouse line, finding reduced number of litters, reduced litter sizes, altered folliculogenesis, and disrupted estrus cyclicity in these animals compared to their wild-type and heterozygous littermates. These data reveal a novel role of UCHL1 in female fertility as well as overall ovarian function, and suggest a potentially essential role for the ubiquitin proteasome pathway in mediating reproductive health.

INTRODUCTION:

In all mammals, the establishment of the ovarian reserve occurs during fetal or neonatal life, although the timing of the process underlying the formation and the exhaustion of the reserve is species-specific. In humans, the ovary is organized by a series of structural and functional rearrangements of germinal and somatic cell lines that both originate and function differently, but are comparative throughout their development [1,2]. As these cell types mutually influence each other through fetal, postnatal, and adult life, any disruption of their balanced relationship is can result in functional abnormalities and infertility [3]. The oocytes present in the adult gonad derive from primordial germ cells (PGCs), which migrate into the gonadal ridges and proliferate as oogonia within germ cell cysts during the fifth week of embryonic life [4–7]. This process, known as oogenesis, continues with the oogonia mitotically dividing into primary oocytes, which then initiate meiotic prophase. Following this, oocytes separate by a process called "cyst break down" and become enclosed in primordial follicles consisting of one oocyte arrested at the diplotene stage of prophase I of meiosis and a layer of somatic pre-granulosa cells. Upon cyst break down, only one-third of the total oocyte population will survive, while the rest succumb to apoptotic cell death. The remaining oocytes form the entire primordial follicle pool available during a female's reproductive lifetime and determine her reproductive capacity. This finite population of follicles remain quiescent until sexual maturation, when follicles are activated and recruited to undergo maturation and ovulation, or die due to follicular atresia [8,9]. In humans, the number of germ cells increases from approximately 600,000 to a peak of 6,800,000 during mid-gestation. At the time of birth, there are approximately 2,000,000 cells present, half of which are atretic [10]. The ovarian reserve continues to steadily decrease over time, and by the age of 7 years, only some 300,000 remain with gradual continued depletion from puberty until menopause [11]. This loss is well-documented and physiologically typical in many species, with mice also experiencing a similar peak in germ cell numbers during late gestation, followed by a significant decline of more than half in the next week of development [7,9,12–16]. As the ovarian reserve represents the entire procreative potential of a female, it is critical to understand its development and the regulation of its formation. It is also essential that this population achieve healthy quiescence after birth, allowing for subsets of these oocytes to be activated, recruited, matured, and potentially ovulated after reproductive maturity. To accomplish these goals, not only must these immature oocytes be available in sufficient numbers, but they must also be competent to communicate with their surrounding somatic cells, and both oocyte and somatic compartments must be appropriately responsive to the effects of gonadotropins and steroid hormones including estrogen, progesterone, follicle stimulating hormone (FSH), and luteinizing hormone (LH) [3].

Proper establishment and function of reproductive processes are dependent on an intricate, yet not fully understood, cascade of events. It has been suggested that the ubiquitin–proteasome pathway plays an important role in many of these processes, including gametogenesis, fertilization, implantation, and embryonic development [17–19]. The ubiquitin-proteasome pathway is responsible for substrate-specific protein degradation and turnover and also plays an important role in eukaryotic cell cycle. Through the concerted actions of a series of enzymes, proteins are marked for proteasomal degradation through the linkage of ubiquitin, a highly conserved polypeptide cofactor. Targets of the ubiquitin-proteasome pathway include protein regulators and transcription factors involved in the regulation of cell division, growth, differentiation, signal transduction, stress response, and apoptosis [20]. Protein ubiquitination is a post-translational modification by which substrate proteins can be targeted for degradation by the 26S proteasome. The reversal of this modification is possible through de-ubiquitination. Deubiquitinating enzymes (DUBs) catalyze the removal of ubiquitin and regulate ubiquitin-mediated pathways and are known to contribute to cell growth, differentiation, oncogenesis, and the regulation of chromosome structure [18,21]. Mutations in the human gene ubiquitin-specific

protease 9 Y chromosome (USP9Y) result in azoospermia and male infertility. Knockout mice lacking certain ubiquitin protein ligases or ubiquitin-conjugating enzymes lead to defects in meiosis, post-meiotic germ-cell development, and male infertility [22–25]. This omnipresent ubiquitin–proteasome system has evident gonadal implications, but its role in female reproductive processes, specifically the development of the ovarian reserve, remains largely unknown.

We identified one such DUB, Ubiquitin C-Terminal Hydrolase L1 (UCHL1, also known as Protein Gene Product 9.5, PGP9.5) as a marker of murine oocytes. Using single-cell-sequencing, our study is one of the first of its kind to be performed on all ovarian cells during the initial establishment of the mouse ovarian reserve. UCHL1 is a multifunctional protein component of the ubiquitin proteasome pathway and was first identified as a member of the ubiquitin carboxyl-terminal hydrolase (UCH) family of DUBs in the late 1980s [26,27]. Since then, UCHL1 has been well-documented as an abundant neuronal protein, constituting 5% of the brain-soluble proteins, although it has also been detected in kidneys, breast epithelium, and reproductive tissues [27–30]. In the brain, UCHL1 plays an important role in the maintenance of axonal and neuronal integrity by removing abnormal proteins via the ubiquitin–proteasome pathway [31–34]. UCHL1 closely interacts with proteins of the neuronal cytoskeleton and regulates synaptic function and long-term potentiation [31,35–39]. Dysfunction of UCHL1 results in impaired motor function and is implicated in variants of common neurodegenerative diseases, such as Parkinson's and Alzheimer's. Additionally, UCHL1 activity protects primary neurons from hypoxia-induced cell death [40,41]. Studies suggest that UCHL1 regulates the cellular pool of free ubiquitin and thus has the potential to influence many ubiquitination-dependent cellular processes, such as proteasomal degradation, DNA damage repair, cell trafficking, cell signaling, endocytosis, and lysosomal degradation. The presence of UCHL1 in various cancer cell lines and tumor tissues, including ovarian, additionally implies that heightened levels of UCHL1 may also promote oncogenic transformation and potentially serve as an oncogene in cancer pathogenesis [27].

While UCHL1 has been primarily studied in the context of neurogenesis, exploration of its role in the ovary is limited. Previous studies using the original Uchl1$^{gad}/_{gad}$ mutant mouse line [42] have demonstrated that truncation of UCHL1 results in an impaired block to polyspermy, with resulting effects on number of litters and number of pups produced by homozygous animals [43]. This role in the block to polyspermy was also observed in higher mammals. Bovine oocytes which had been subjected to chemical inhibition of UCHL1 followed by *in vitro* fertilization resulted in zygotes with much higher rates of polyspermy compared to controls [18]. Additional work on UCHL1 function in mammalian oocytes similarly utilized chemical inhibitors to test the developmental effects on mouse and rhesus oocytes [44], observing similar consequences on aberrant fertilization, effects which have also been observed in porcine oocytes [19]. Finally, initial studies by Yan-Qiong et al [45] have shown increased UCHL1 expression in morphologically abnormal oocytes in pre-pubertal mouse ovaries, though a mechanism of UCHL1-mediated oocyte survival or loss has not been demonstrated.

Our study aimed to better understand the oocyte- and ovary-intrinsic roles of UCHL1 expression, as well as the systemic effects of UCHL1 loss on murine female fertility. In this work, we have demonstrated for the first time that UCHL1 is a marker of all post-natal murine oocytes, and that its loss results in impaired ovarian function, estrus cyclicity, response to hormonal stimulation, and fecundity. Future studies will be critical in dissecting the specific molecular mechanisms of UCHL1, as well as a better understanding of its interacting partners and role in protein homeostasis.

RESULTS:

***Uchl1* is highly expressed specifically in oocytes within the mouse ovary, with protein localization in oocytes of all stages**

In an effort to identify and profile the dynamic gene expression changes that take place during murine ovarian reserve formation, we collected mouse ovaries at several time points to span the establishment of the ovarian reserve (embryonic day 18.5, E18.5, and postnatal days (PND) 1, 3, and 5; n=22, 24, 15, 10 animals respectively). By choosing these time points, we expected to capture oocytes still within ovarian cysts, as well as oocytes undergoing cyst breakdown, and oocytes which are later comprising primordial follicles. For each time point, 4–5,000 cells per mouse were processed through the 10X Genomics Chromium System using standard protocols for single cell RNA sequencing (scSEQ). Libraries were sequenced to an average depth of 1.3 billion reads; on average, 93.1% of reads mapped to the reference genome. After standard data processing, we obtained gene expression profiles for approximately 1100 cells per library (Figure 1A), of which a total of only 70, or about 2%, were germ cells, identified by *Dazl* and *Ddx4* expression (Supplementary Figure 1). While most of the cells in our data set were ovarian somatic cells, this germ cell retention limitation is not unique to this study, with other recent studies also demonstrating comparatively reduced germ cell representation compared to somatic cell representation [46].

We were able to identify globally distinguishing genes in the oocyte population, or genes which are highly and specifically expressed in the germ cells of the developing ovarian reserve. Oocytes selected by expression of the germ cell markers *Dazl* and *Ddx4* (Supplementary Figure 1) were further analyzed to identify novel gene expression dynamics. Our analysis revealed a list of the top 20 oocyte-specific factors (Figure 1A), the vast majority of which are already well-characterized for expression and function, including *Dazl*, meiosis regulators *Sycp1, Sycp3, Syce3, Hormad1*, and *Smc1b* [47]; transcriptional regulators *Figla* [48–50] and *Taf7l* [51]; and retrotransposon regulators *Mov10l1* [52] and *Mael* [53,54]. While these serve as excellent positive controls for the fidelity of our study, our aims to identify novel regulators resulted in further analysis of the 20th most highly-expressed oocyte-specific gene identified in our study, *Uchl1* (Figure 1B).

Due to low oocyte yield in our dataset, we also mined existing data sets to independently verify our *Uchl1* oocyte expression data. In the PND0 murine ovarian dataset from Wang et al [55], the authors retained nearly 3000 oocytes for their analysis, allowing us to correlate *Uchl1* expression with other known regulators of oocyte development. Correlation analysis of *Uchl1* with oocyte-specific transcriptional regulators *Figla*, *Sohlh1*, and *Lhx8* revealed significant correlations between the expression of both genes (r=0.7895, r=0.7700, and r=0.7074 respectively; Supplementary Figure 2), further suggesting that *Uchl1* may be playing a key role in oocyte development at the same time as these known master regulators. Interestingly, recent work has demonstrated a genetic relationship between FIGLA and SOHLH1 and UCHL1 with *Uchl1* mRNA expression reduced nearly 50% in *Figla*-knockout ovaries ($p=3.4xe^{-13}$) and nearly 90% *Sohlh1*-knockout ovaries ($p=6.3xe^{-133}$) [56]. Significant change in *Uchl1* expression was not, however, observed in *Lhx8*-knockout ovaries, despite the expression correlation observed in our analysis. Overall, this speaks to a network of oocyte-specific regulators of a variety of functions, working in concert to promote establishment of a healthy and functional ovarian reserve.

UCHL1 has been studied cursorily in the context of oogenesis, though these studies utilized other model systems [19], knockdowns instead of genetic mutants [18,44], or obsolete UCHL1-deficient mouse lines

which may not reflect loss of function of the protein [42,43]. Furthermore, UCHL1 has never been studied in the context of ovarian reserve formation, leading us to explore its expression and localization in this context. Wild-type mouse ovaries were obtained from a variety of perinatal (Figure 2) as well as juvenile and adult (Figure 3) time points and immune-stained for UCHL1. Perinatal mouse ovaries were also stained with an antibody against TRA98, an early germ cell marker [57], allowing us to observe the initiation of UCHL1 expression in this population. This staining revealed a protein localization pattern that is consistent with the scSEQ mRNA data, with oocyte-specific expression through all stages of follicle development. While a low level of *Uchl1* expression was observed in some somatic cells in our scSEQ dataset, this was not observed at the protein level, and may represent either untranslated mRNA, or potential contamination from cell-free RNA [58]. From this staining, we also observed UCHL1 co-localization with early oocyte marker TRA98. Interestingly, it appears that at E18.5, only a subset of TRA98-positive oocytes are UCHL1-positive, suggesting an intriguing possibility that UCHL1 may represent a part of a survival signature in oocytes, as it is expressed in a subset of oocytes at the peak of perinatal oocyte attrition [6–9], and oocytes which remain after this wave of attrition are nearly all UCHL1-positive (Figure 2). This ubiquitous, oocyte-specific UCHL1 expression remains throughout juvenile and adult life, including in reproductive-aged 8 month old mice, though at this time, the fibrosis of the ovary also non-specifically binds the secondary antibody (Figure 3). Importantly, and as expected, UCHL1 knockout ovaries have no detectable UCHL1 expression (Supplemental Figure 3).

UCHL1 knockout mice are severely sub-fertile, with heterozygous mice exhibiting a less severe reduction in fertility

To better understand the role that UCHL1 may be playing mammalian oocyte development, we obtained a UCHL1-heterozygous mouse line (B6.C-Uchl1^{gad-J}/J), which we bred to obtain all genotypes: B6.C-Uchl1^{J}/J ("wild-type"), B6.C-Uchl1^{gad-J}/J ("heterozygous"), or B6.C-Uchl1^{gad-J}/$^{gad-J}$ ("knockout"). Mice of all genotypes (n=3 for both wild-type and knockout, n=4 for heterozygotes) were paired with verified C57BL/6J male breeders in single-breeding-pair cages at 6 weeks of age. Mice were monitored for the presence of copulation plugs, evidence of pregnancy, the birth of pups, and the number of live pups per litter. Knockout mice appear to breed normally with repeated observation of copulation plugs (data not shown). As UCHL1 knockout mice develop severe motor neuron dysfunction between 6-7 months of age, breedings were only maintained until 5 months of age, at which time all mice were euthanized. Severe sub-fertility in knockout females was demonstrated with significantly fewer litters than wild-type animals (0.667 litters vs. 4.333 litters, respectively, p=0.042). Knockout animals also produce significantly fewer pups per litter than wild-type animals (2.500 pups v.s 8.769 pups, respectively, p=0.0002), as well as fewer pups per litter than heterozygous animals (2.500 pups v.s 6.625 pups, respectively, p=0.008). Heterozygous animals also demonstrate a non-significant trend toward reduced litters and litter sizes (Figure 4).

UCHL1 knockout mice demonstrate estrus cyclicity disruption as well as reduced response to ovarian stimulation

The severe subfertility seen in knockout animals could be correlated with disrupted estrus cyclicity, reduced follicle abundance or recruitment, and reduced ovulations in these animals. Consistent with this hypothesis, estrus cyclicity analysis in all genotypes of mice revealed significantly disrupted cycles in both knockout and heterozygous animals. Mice were assessed for vaginal cytology daily for two weeks starting at 40 days of age, and percentage of time spent in each cycle stage was averaged between animals in a genotype (n=3 for wildtype, n=6 for heterozygotes, and n=5 for knockouts). Interestingly, both heterozygotes and knockouts spent significantly less time in the follicular phase of proestrus

(p=0.0145 and p=0.0085 respectively) and spent significantly more time in the secretory phase of diestrus (p=0.0434 and p=0.0456 respectively) than wild-type animals (Figure 5A). Additionally, knockout animals trended towards increased time spent in estrus, with several animals spending greater than 5 days in uninterrupted estrus, though this average did not reach statistical significance.

In addition to impaired hormonal cyclicity, knockout animals are also significantly less responsive to ovulation induction (Figure 5B). At 28 days of age, animals of all genotypes (n=13 wild-type, 14 heterozygous, 3 knockout animals) were given intraperitoneal injections of 5IU Pregnant Mare Goat Serum (PMSG) followed 48 hours later by intraperitoneal injections of 5IU Human Chorionic Gonadotropin (HCG). Super-ovulated cumulus-oocyte complexes were collected from the ampullas of all mice 12 hours after HCG injection. Oocytes were stripped by brief incubation in hyaluronidase and counted, with counts per animals averaged per genotype. Significantly fewer oocytes were recovered from knockout animals compared to their heterozygous or wild-type counterparts (an average of 7, 23.2, and 27.8 oocytes per animal, respectively, p=0.050), despite ovarian follicle counts appearing indistinguishable at this same time point (Figure 6A).

UCHL1-heterozygous and -knockout ovaries contain normal follicle densities early in life and produce normal Anti-Mullerian Hormone, with ovarian function becoming compromised by middle age

To better understand the ovary-intrinsic effects of UCHL1 loss, ovaries from all genotypes of mice were collected at 1 month and 5 months of age, paraffin-embedded, sectioned, and stained with hematoxylin and eosin for follicle staging. Ovarian follicle counts were quantified using two sections on every fourth slide of sectioned ovary to capture all follicle stages without over-counting of larger follicles. Follicle counts were normalized to the section area to account for size differences between different ovaries. Ovarian weights were also obtained from 5-month-old animals and compared to body weight as a readout of ovarian volume.

At 1 month of age, all genotypes possess similar densities of all follicle stages, suggesting initially normal development and maturation of ovarian follicles, despite qualitative appreciation of increased degenerating or atretic follicles in knockout ovaries (Figure 6A, C-E). While heterozygotes possessed significantly more primordial follicles than knockout animals per unit area at this age (p=0.0308; n=8 wild-type, 6 heterozygous, 6 knockout animals), this effect was not observed in wild-type or knockout animals, suggesting that this may be a result of inter-animal variation. As an independent assessment of ovarian follicle endowment, additional mice were collected at 2.5 months, with whole blood collected for serum analysis of Anti-Mullerian Hormone (AMH). AMH is currently the gold standard for measuring oocyte endowment, as it is produced by the granulosa cells of growing follicles [59]. Consistent with our 1 month follicle density data, no differences were observed in AMH serum concentrations between genotypes at 2.5 months of age (n=3 wild-type, 7 heterozygous, 6 knockout animals; Figure 6B).

Interestingly, however, UCHL1 knockout ovaries begin to demonstrate ovarian dysfunction just a few months later, with decreased ovarian volume (Figure 7B,C) as well as altered follicle densities compared to wild-type and knockout animals (n=4 wild-type, 2 heterozygous, 4 knockout animals; Figure 7A, D-F). While primordial follicle densities are the only significantly enriched follicle stage in 5-month-old knockout ovaries (p=0.0206 vs. wild-type animals, and p=0.0443 vs. heterozygous animals), densities of all follicle stages trend towards greater enrichment in knockout ovaries. This is surprising, given the reduced ovarian volume at this time, with knockout ovaries being significantly smaller than wild-type ovaries when normalized for body weight (p=0.050; n=3 wild-type, 5 heterozygous, 5 knockout animals;

Figure 7B,C). While this is an unexpected result given the retained follicle density in these animals, these data suggest a potential deficit in oocyte maturation or folliculogenesis.

DISCUSSION:

The mammalian ovarian reserve directly impacts ovarian function and endocrine balance, making the health of this cell population not only essential for fertility but also female health-span and lifespan. The regulation of oocyte endowment, development, maturation, and resulting endocrine function rely on myriad molecular mechanisms to regulate these developmental transitions, including transcriptional regulation, post-transcriptional and translational mechanisms, and protein homeostasis. As oocytes must remain arrested in the ovary from the time of initial perinatal quiescence to the time of activation weeks to months later in the mouse, or years to decades later in the human, ensuring adequate protein supply, homeostasis, and turnover is likely essential for the developmental success of this population. UCHL1 is a deubiquitinating enzyme known to regulate free cellular mono-ubiquitin, turnover of ubiquitin pro-proteins, and protein abundance and stasis [27]. In this work, we have determined the effects of UCHL1 loss on mouse ovarian development and function, finding an essential role for UCHL1 in the proper balance of mouse folliculogenesis, with loss resulting in severely impaired fertility and hormone responsiveness of the ovary.

Our finding of reduced litter numbers and litter sizes in B6.C-Uchl1$^{gad\text{-}J}$/$^{gad\text{-}J}$ ovaries is consistent with previous work using the original Uchl1^{gad}/$_{gad}$ truncation mutant, but contrasts with other findings from this study. Sekiguchi et al [43] found that while Uchl1^{gad}/$_{gad}$ animals were significantly sub-fertile, they did not possess visually abnormal ovaries, though follicle abundance was not quantified, and were able to ovulate similar numbers of oocytes compared to wild-type animals when hormonally stimulated. Instead, the authors attribute the observed sub-fertility to a loss of the block to polyspermy, resulting in failed embryo development. Indeed, B6.C-Uchl1$^{gad\text{-}J}$/$^{gad\text{-}J}$ animals may suffer similar effects on fertilization and early embryo development, though our study also elucidates the ovary-intrinsic effects of UCHL1 loss. The observed differences in phenotype between these two mouse lines may be a result of differences in the site of mutation, as the Uchl1^{gad}/$_{gad}$ mutation was produced by an in-frame deletion causing UCHL1 truncation of 42 residues [42]. In contrast, the currently available B6.C-Uchl1$^{gad\text{-}J}$/$^{gad\text{-}J}$ mutation resulted from a spontaneous mutation in a BALB/cJ mouse line at Jackson Laboratory [60]. Back-crossing of this mutation onto a pure C57BL/6J background revealed the mutation to ablate a large intragenic region, ultimately resulting in the truncation of the final 78 residues of the protein. Phenotypic differences may also result from the contribution of different strain backgrounds, as the Uchl1^{gad}/$_{gad}$ animals studied in the Sekiguchi work were autosomal recessive F1 hybrid mutants resulting from a cross of CBA and RFM animals, while B6.C-Uchl1$^{gad\text{-}J}$/$^{gad\text{-}J}$ animals are maintained on a pure C57bl/6J background.

Perhaps most intriguing is that UCHL1 knockout ovaries at 1 month of age initially appear to contain comparable follicle densities to their wild-type and heterozygous counterparts, though many of these follicles appear to be morphologically degenerative and likely of poor quality. During mid-reproductive life, despite reduced ovarian size, knockout ovaries have significantly increased follicle densities compared to age-matched ovaries of other genotypes, suggesting a potential delay in follicle maturation or lack of sensitivity to atresia, resulting in follicle retention. Indeed, even when hormonally stimulated, knockout animals at 1 month of age ovulate fewer oocytes than their littermates of other genotypes, suggesting reduced responsiveness to normal hormonal stimuli. This hypothesis gains further support from the observation that knockout animals do not estrus cycle normally, with significantly reduced time spent in the follicular phase, and significantly more time spent in the secretory phase.

These investigations are not without their limitations. We cannot rule out that loss of UCHL1 expression in the brain contributes to these observed endocrine effects, as the hypothalamic-pituitary-ovarian axis creates an inextricable feedback loop between the function of the ovary and the endocrine function of the brain and pituitary gland. Given that UCHL1 is expressed in gonadotropes of the pituitary gland [61], the lack of robust hormone responsiveness in knockout animals is not entirely surprising, and these effects are difficult to parse apart from ovarian effects, as the axis is complex and inter-dependent. Interestingly, other mutant mice with estrus cyclicity defects, including a short proestrus phase, include gonadotropin-releasing hormone (*mGnRH*) mutants [62] as well as DMX Like 2 (*Dmxl2*) mutants, which also affect GnRH signaling [63]. The shorter proestrus phase in these mutant animals, much like that observed in the UCHL1 mutants in this study, suggests that disrupted GnRH production, signaling, and responsiveness could contribute to the altered estrus cyclicity and reduced response to ovulation induction we observe. This is particularly relevant, as GnRH is known to stimulate the pituitary gland to produce follicle stimulating hormone and luteinizing hormone, which are essential for ovulation [64]. Future studies utilizing an oocyte-specific UCHL1-conditional mouse line will assist us in the endeavors to resolve neuroendocrine versus ovarian effects of UCHL1 loss, and will allow us to better assess reproductive fitness in animals which do not suffer premature motor neuron decline and death.

UCHL1 loss may also have a more direct effect on oocyte health and developmental potential by directly regulating the protein abundance, composition, and turnover in both resting and maturing oocytes. Loss of UCHL1 in Uchl1$^{gad}/_{gad}$ oocytes has been shown to reduce free mono-ubiquitin in these cells, likely directly affecting the ability of these oocytes to mature and grow properly [18]. Future studies will further elucidate the underlying biochemical mechanisms of UCHL1 influence in these cells, though the literature provides lessons from the demonstrated role of UCHL1 in the quiescence and differentiation of developing male germ cells. Studies of testis development and function in the original UCHLl1$^{gad}/_{gad}$ animals revealed that while testis volume is initially normal at 12-weeks-of-age in homozygous mutants, testis volume significantly decreased with age, with an approximately 30% reduction in size by 25 weeks of age, accompanied by reduced spermatogonial stem cell (SSC) proliferation at this same time [65]. This testicular phenotype is much like that we observe in the ovary, with initially normal size, but loss of volume with age. Interestingly, follow-up studies from these authors demonstrated an increase in premeiotic germ cells in juvenile UCHLl1$^{gad}/_{gad}$ mice, despite reduction in all stages of germ cells later in life, suggesting that UCHL1 may help to regulate both sensitivity to apoptosis as well as developmental competence [66]. If this were to be true for ovarian populations as well, it may explain why we observe degenerating follicles in UCHL1 knockout animals, but without catastrophic loss of follicle abundance. Furthermore, recent studies from Alpaugh et al utilizing a different UCHL1 mouse line, Uchl1^{tm1Dgen}, demonstrated that UCHL1-deficient SSCs are less competent to repopulate busulfan-ablated testes, exhibiting only about 20% regenerative capacity compared to 60% in their wild-type counterparts [67]. The authors posit that this lack of developmental potential may result from impaired mitochondrial metabolism of UCHL1-deficient SSCs, and directly result from altered mitochondrial protein turnover. These findings are consistent with recent work utilizing chemical inhibition of UCHL1 in *in vitro* matured mouse oocytes, demonstrating aberrant maturation resulting from altered mitochondrial metabolism [68].

It will be enlightening to explore the intersection of germ cell protein homeostasis, cell metabolism, and developmental competence in future studies. By better understanding the ways in which UCHL1 functions in the development of the oocytes and, therefore, the ovary, we will better understand the ways in which the ubiquitin-proteasome pathway can contribute to protein turnover in highly dynamic cells, as well as govern the ability of those cells to differentiate and develop properly.

429 **METHODS:**
430
431 **Animals**
432 C57bl/6 (wild-type) and B6.C-*Uchl1*$^{gad\text{-}J}$/J [60] were obtained from the Jackson Laboratory (strain #
433 024355). B6.C-Uchl1 J/J ("wild-type"), B6.C-Uchl1$^{gad\text{-}J}$/J ("heterozygous"), or B6.C-Uchl1$^{gad\text{-}J}$/$_{gad\text{-}J}$
434 ("knockout") mice were generated by mating UCHL1 heterozygous male and female mice. Offspring
435 were genotyped by PCR analysis of ear-snip genomic DNA amplifying the region targeted by homologous
436 recombination using genotyping protocols established by the Jackson Laboratory. All animal protocols
437 were reviewed and approved by Brown University Institutional Animal Care and Use Committee and
438 were performed in accordance with the National Institutes of Health Guide for the Care and Use of
439 Laboratory Animals (# 19-07-0001). All animal protocols were all reviewed and acknowledged by the
440 Lifespan University Institutional Animal Care and Use Committee (# 1668974-1).
441
442 **Generation of Ovarian Single Cell Libraries**
443 Ovaries were collected from mice at embryonic day 18.5 (E18.5), and postnatal days (PND) 1, 3, and 5
444 and pooled to generate pools of 1 million cells per time-point (E18.5 n=47 ovaries, PND1 n=29 ovaries,
445 PND3 n=25 ovaries, PND5 n=8 ovaries). Ovaries were dissociated by incubation in 750 µL 0.25% Trypsin-
446 EDTA for 30 min at 37 °C with rotation. Cells were then spun at 500 g for 5 min, and resuspended in 150
447 µL 7 mg/mL DNase I and gently pipetted to disperse cells. Cells were incubated for 5 min at room
448 temperature, and then DNase I activity was quenched by addition of 1 mL PBS + 10% Knockout Serum
449 Replacement. Cells were filtered through a 40 µM filter and spun again at 500 g for 5 min. The resulting
450 cell pellets were counted and resuspended in freezing media (70% DMEM, 20% Knockout Serum
451 Replacement, 10% DMSO) and stored at -80 °C in cryotubes.
452
453 Cell preparation were then submitted to Genewiz for 10X Genomics scSEQ on the 10X Genomics
454 Chromium System. Libraries were sequenced to an average depth of 394M reads (range 372M-423M);
455 on average, 93% of reads (range 88%-95%) mapped to the reference genome. Initial bioinformatics
456 analyses were conducted at GENEWIZ, LLC. Loupe Cell Browser 2.0.0 was used for downstream analysis
457 of ovarian somatic cells and oocytes at all time points and visualization with t-distributed stochastic
458 neighbor embedding (tSNE) plots.
459
460 Data availability: The single-cell RNAseq data have been deposited in the NCBI Gene Expression Omnibus
461 (GEO) and are accessible through accession number GSE186843.
462
463 **Single-cell RNA seq (scSEQ) data analysis [69]**
464 The PND0 sample SRP214792 from GEO Series GSE134339 was downloaded from NCBI SRA onto Brown
465 University's high-performance computing cluster at the Center for Computation and Visualization. The
466 fastq files were aligned using Cell Ranger (v 5.0.0) count to the mm10 genome. The resulting "filtered
467 feature bc matrix" was used as input for Seurat (v 3.9.9) in RStudio (R v 4.0.2) [69]. Seurat was used to
468 select for *Ddx4*-positive (Ddx4 > 0), high-quality (nFeature_RNA > 100, nFeature_RNA < 7000, nCount <
469 40000, percent mitochondrial genes < 15%) oocytes. To obtain gene counts, the Seurat function
470 "GetAssayData" under the slot "counts" was used. Normalized gene expression counts for *Uchl1*
471 compared to *Sohlh1*, *Figla*, and *Lhx8* were plotted in Graphpad Prism and a linear regression applied.
472
473 **Immunofluorescence**
474 Wild-type ovaries were collected at E18.5, PND0, PND1, PND3, 3 weeks, and 12 weeks of age, cleaned of
475 excess fat, and fixed in 0.1% formalin solution overnight before dehydration and embedding in paraffin.
476 Fixed ovaries were sectioned at 5 µm onto glass slides by the Brown University Molecular Pathology

Core. To stain, sections were de-paraffinized by 3x, 5 minute washes in Histoclear followed by rehydration in 100% ethanol (2x, 5 minutes), 95% ethanol (2x, 5 minutes), 70% ethanol (1x, 5 minutes), water (1x, 5 minutes). Sections were then incubated in boiling antigen retrieval buffer (10 mM sodium citrate, 0.05% Tween-20, pH 6.0) for 20 minutes and left to cool. Sections were washed 3x, 5 minutes in 1X PBS + 0.1% Triton-X (PBST). Tissue sections were then incubated in blocking buffer [3% Goat Serum (Sigma), 1% Bovine Serum Albumin (Sigma), and 0.5% Triton-X (Fisher Scientific) in 1X PBS] and stained by incubation with primary antibodies against UCHL1 (Proteintech #14730-1-AP, 1:100) and TRA98 (Abcam #ab82527; 1:100 overnight at 4 °C. The following day, slides were washed 3x, 5 minutes in PBST and then incubated with secondary antibodies raised in goat against mouse (594 nm) and rabbit (488 nm) at 1:500 for 1 hour at 37 °C. A secondary antibody-only control was included to assess background staining. Sections were further stained with DAPI to visualize nuclei, mounted and analyzed on a Nikon TE2000e inverted epifluorescence microscope. For a given set of antibodies, images were exposed equivalently for all samples from different time points to generate images for relative comparison of intensity over time.

Fertility Trials

To assess female fertility in all genotypes of B6.C-*Uchl1*$^{gad\text{-}J}$/J mice, controlled fertility trials were performed. terms B6.C-Uchl1 J/J, B6.C-Uchl1$^{gad\text{-}J}$/J, or B6.C-Uchl1$^{gad\text{-}J}$/$_{gad\text{-}J}$ females were housed with wild-type C57BL/6J males, both at 6 weeks of age. All animals were housed in single breeding pairs with love huts, and monitored for signs of copulation, pregnancy, and birth of pups. Number and sizes of litters were recorded. As *Uchl1*-null mice develop severe motor dysfunction by 6-7 months of age, all breedings were disbanded at 20 weeks of age, and compared between genotypes.

Vaginal Cytology

Daily vaginal smear cytology was performed over the course of two weeks to determine estrous cyclicity, beginning at 6 weeks of age on virgin females. Briefly, the vagina of each mouse was flushed with a small volume of sterile saline solution and then mixed on a glass slide with Toluidine Blue O dye [70]. Slides were visualized on an EVOS M5000 Fluorescence Imaging System and were classified as in proestrus, estrus, or metestrus/diestrus based on the majority cell type present in the vaginal sample [70]. The percentage of time spent in each sub-stage was quantified per mouse and averaged per genotype. Following estrus cycling, mice were allowed to recover for two weeks, at which point mice were sacrificed and ovaries collected for analysis of ovary weights versus body weights.

Ovarian Histology

Ovaries were removed, cleaned of excess fat and bursal sac, and fixed in 1:10 formalin solution overnight. Standard paraffin embedding, 5 µM sectioning, and hematoxylin-and-eosin staining were performed. Slides were visualized on an EVOS M5000 Fluorescence Imaging System and images of all fields of a single section were captured. Ovarian follicle counts were quantified using two sections on every fourth slide of sectioned ovary to capture all follicle stages without over-counting of larger follicles. Follicle counts were normalized to section area to account for size differences between different ovaries.

Super-ovulation

Mice at 4 weeks of age were super-ovulated by standard protocols [71]. Briefly, mice were injected intraperitoneally with 5 IU Pregnant Mare Goat Serum (PMSG; Prospec Bio). Forty-eight hours later, the same mice were intraperitoneally injected with 5 IU Human Chorionic Gonadotropin (HCG; Prospec Bio). Twelve hours later, mice were euthanized and ovaries and oviducts collected. Ovulated cumulus-oocyte

complexes were released from the ampulla of the oviduct and counted per mouse. Number of oocytes per mouse were averaged between genotypes and compared.

Serum hormone analysis

Whole blood was collected from mice at 80 days of age by cardiac puncture. Blood was collected into serum separator tubes, allowed to clot for 30 minutes, then spun at 3000g for 15 min at 4 °C. The supernatant was collected as serum for analysis. Serum was sent to the University of Virginia Ligand Assay & Analysis Core of the Center for Research in Reproduction for analysis of Anti-Mullerian Hormone and Testosterone serum concentrations.

Statistical Analysis

All statistical analyses were performed in GraphPad Prism, and all data assessed for normal distribution. Fecundity, follicle count, and estrus cyclicity analyses were performed using 2-way ANOVA with multiple comparisons. Analysis of litter and ovary weights were performed using 1-way ANOVA with multiple comparisons. Serum AMH analyses were also performed using 1-way ANOVA.

ACKNOWLEDGEMENTS:

The authors would like to thank The Program in Women's Oncology of Women and Infants Hospital and Swim Across America. This work was also supported by University of Virginia Center for Research in Reproduction Ligand Assay and Analysis Core supported by the Eunice Kennedy Shriver NICHD Grant R24 HD102061. We are grateful to the NICHD for their generous support through award 1F31HD097933 to MAG. Part of this research was conducted using computational resources at the Center for Computation and Visualization at Brown University. The authors thank the Freiman and Ribeiro laboratories for their helpful feedback on this project.

AUTHOR CONTRIBUTIONS:

All writing of the manuscript was done by MFW and KJG. Experimental designed was performed by MFW, MCHO, and KJG. Experiments for the manuscript were carried out by MFW, MCHO, PD, AG, and KJG. Analysis for the manuscript was performed by MFW, MAG, PD, and KJG.

DATA AVAILABILITY:

The scSEQ data have been deposited in the NCBI Gene Expression Omnibus (GEO) at https://www.ncbi.nlm.nih.gov/geo/query/acc.cgi?acc=GSE186843 and are accessible through accession number GSE186843.

CONFLICT OF INTEREST:

The authors declare that there are no conflicts of interest.

FUNDING:

This work was supported in part by the NIH P20 GM121298 (COBRE for Reproductive Health) grant as well as funding from Swim Across America.

REFERENCES:

1. Makabe S, Naguro T, Nottola SA, Pereda J, Motta PM. Migration of germ cells, development of the ovary, and folliculogenesis. In: Familiari G, Makabe S, Motta PM, editors. Ultrastructure of the ovary. Boston, MA: Springer US; 1991. pp. 1–27. doi:10.1007/978-1-4615-3944-5_1
2. Motta P, Makabe S, Nottola S. The ultrastructure of human reproduction. I. The natural history of the female germ cell: origin, migration and differentiation inside the developing ovaryNo Title. Hum Reprod Update. 1997;3: 281–295.
3. Franchi LL, Baker TG. Oogenesis and Follicular Growth . In: Hafez ESE, editor. Human Reproduction: Conception and Contraception . 1973. pp. 53–83.
4. Monniaux D, Clément F, Dalbiès-Tran R, Estienne A, Fabre S, Mansanet C, et al. The ovarian reserve of primordial follicles and the dynamic reserve of antral growing follicles: what is the link? Biol Reprod. 2014;90: 85. doi:10.1095/biolreprod.113.117077
5. Monniaux D. Driving folliculogenesis by the oocyte-somatic cell dialog: Lessons from genetic models. Theriogenology. 2016;86: 41–53. doi:10.1016/j.theriogenology.2016.04.017
6. Pepling ME. From primordial germ cell to primordial follicle: mammalian female germ cell development. Genesis. 2006;44: 622–632. doi:10.1002/dvg.20258
7. Grive KJ, Freiman RN. The developmental origins of the mammalian ovarian reserve. Development. 2015;142: 2554–2563. doi:10.1242/dev.125211
8. Pepling ME. Follicular assembly: mechanisms of action. Reproduction. 2012;143: 139–149. doi:10.1530/REP-11-0299
9. Grive KJ. Pathways coordinating oocyte attrition and abundance during mammalian ovarian reserve establishment. Mol Reprod Dev. 2020;87: 843–856. doi:10.1002/mrd.23401
10. Geber S, Megale R, Vale F, Lanna AMA, Cabral ACV. Variation in ovarian follicle density during human fetal development. J Assist Reprod Genet. 2012;29: 969–972. doi:10.1007/s10815-012-9810-2
11. Baker TG. A quantitative and cytological study of germ cells in human ovaries. Proc R Soc Lond, B, Biol Sci. 1963;158: 417–433. doi:10.1098/rspb.1963.0055
12. Morita Y, Maravei DV, Bergeron L, Wang S, Perez GI, Tsutsumi O, et al. Caspase-2 deficiency prevents programmed germ cell death resulting from cytokine insufficiency but not meiotic defects caused by loss of ataxia telangiectasia-mutated (Atm) gene function. Cell Death Differ. 2001;8: 614–620. doi:10.1038/sj.cdd.4400845
13. Ford EA, Beckett EL, Roman SD, McLaughlin EA, Sutherland JM. Advances in human primordial follicle activation and premature ovarian insufficiency. Reproduction. 2020;159: R15–R29. doi:10.1530/REP-19-0201
14. Jones RL, Pepling ME. Role of the antiapoptotic proteins BCL2 and MCL1 in the neonatal mouse ovary. Biol Reprod. 2013;88: 46. doi:10.1095/biolreprod.112.103028
15. Myers M, Morgan FH, Liew SH, Zerafa N, Gamage TU, Sarraj M, et al. PUMA regulates germ cell loss and primordial follicle endowment in mice. Reproduction. 2014;148: 211–219. doi:10.1530/REP-13-0666
16. Pepling ME, Spradling AC. Mouse ovarian germ cell cysts undergo programmed breakdown to form primordial follicles. Dev Biol. 2001;234: 339–351. doi:10.1006/dbio.2001.0269
17. Sutovsky P. Review: Sperm-oocyte interactions and their implications for bull fertility, with emphasis on the ubiquitin-proteasome system. Animal. 2018;12: s121–s132. doi:10.1017/S1751731118000253
18. Susor A, Liskova L, Toralova T, Pavlok A, Pivonkova K, Karabinova P, et al. Role of ubiquitin C-terminal hydrolase-L1 in antipolyspermy defense of mammalian oocytes. Biol Reprod. 2010;82: 1151–1161. doi:10.1095/biolreprod.109.081547

19. Susor A, Ellederova Z, Jelinkova L, Halada P, Kavan D, Kubelka M, et al. Proteomic analysis of porcine oocytes during in vitro maturation reveals essential role for the ubiquitin C-terminal hydrolase-L1. Reproduction. 2007;134: 559–568. doi:10.1530/REP-07-0079
20. Tu Y, Chen C, Pan J, Xu J, Zhou Z-G, Wang C-Y. The Ubiquitin Proteasome Pathway (UPP) in the regulation of cell cycle control and DNA damage repair and its implication in tumorigenesis. Int J Clin Exp Pathol. 2012;5: 726–738.
21. Chung CH, Baek SH. Deubiquitinating enzymes: their diversity and emerging roles. Biochem Biophys Res Commun. 1999;266: 633–640. doi:10.1006/bbrc.1999.1880
22. Roest HP, van Klaveren J, de Wit J, van Gurp CG, Koken MH, Vermey M, et al. Inactivation of the HR6B ubiquitin-conjugating DNA repair enzyme in mice causes male sterility associated with chromatin modification. Cell. 1996;86: 799–810. doi:10.1016/s0092-8674(00)80154-3
23. Suzumori N, Burns KH, Yan W, Matzuk MM. RFPL4 interacts with oocyte proteins of the ubiquitin-proteasome degradation pathway. Proc Natl Acad Sci USA. 2003;100: 550–555. doi:10.1073/pnas.0234474100
24. Dickins RA, Frew IJ, House CM, O'Bryan MK, Holloway AJ, Haviv I, et al. The ubiquitin ligase component Siah1a is required for completion of meiosis I in male mice. Mol Cell Biol. 2002;22: 2294–2303. doi:10.1128/mcb.22.7.2294-2303.2002
25. Sun C, Skaletsky H, Birren B, Devon K, Tang Z, Silber S, et al. An azoospermic man with a de novo point mutation in the Y-chromosomal gene USP9Y. Nat Genet. 1999;23: 429–432. doi:10.1038/70539
26. Wilkinson KD, Lee KM, Deshpande S, Duerksen-Hughes P, Boss JM, Pohl J. The neuron-specific protein PGP 9.5 is a ubiquitin carboxyl-terminal hydrolase. Science. 1989;246: 670–673. doi:10.1126/science.2530630
27. Hurst-Kennedy J, Chin L-S, Li L. Ubiquitin C-terminal hydrolase l1 in tumorigenesis. Biochem Res Int. 2012;2012: 123706. doi:10.1155/2012/123706
28. Schumacher U, Mitchell BS, Kaiserling E. The neuronal marker protein gene product 9.5 (PGP 9.5) is phenotypically expressed in human breast epithelium, in milk, and in benign and malignant breast tumors. DNA Cell Biol. 1994;13: 839–843. doi:10.1089/dna.1994.13.839
29. Bishop P, Rocca D, Henley JM. Ubiquitin C-terminal hydrolase L1 (UCH-L1): structure, distribution and roles in brain function and dysfunction. Biochem J. 2016;473: 2453–2462. doi:10.1042/BCJ20160082
30. Bradbury JM, Thompson RJ. Immunoassay of the neuronal and neuroendocrine marker PGP 9.5 in human tissues. J Neurochem. 1985;44: 651–653. doi:10.1111/j.1471-4159.1985.tb05461.x
31. Liu H, Povysheva N, Rose ME, Mi Z, Banton JS, Li W, et al. Role of UCHL1 in axonal injury and functional recovery after cerebral ischemia. Proc Natl Acad Sci USA. 2019;116: 4643–4650. doi:10.1073/pnas.1821282116
32. Liu Y, Fallon L, Lashuel HA, Liu Z, Lansbury PT. The UCH-L1 gene encodes two opposing enzymatic activities that affect alpha-synuclein degradation and Parkinson's disease susceptibility. Cell. 2002;111: 209–218. doi:10.1016/s0092-8674(02)01012-7
33. Chen F, Sugiura Y, Myers KG, Liu Y, Lin W. Ubiquitin carboxyl-terminal hydrolase L1 is required for maintaining the structure and function of the neuromuscular junction. Proc Natl Acad Sci USA. 2010;107: 1636–1641. doi:10.1073/pnas.0911516107
34. Bilguvar K, Tyagi NK, Ozkara C, Tuysuz B, Bakircioglu M, Choi M, et al. Recessive loss of function of the neuronal ubiquitin hydrolase UCHL1 leads to early-onset progressive neurodegeneration. Proc Natl Acad Sci USA. 2013;110: 3489–3494. doi:10.1073/pnas.1222732110
35. Sakurai M, Sekiguchi M, Zushida K, Yamada K, Nagamine S, Kabuta T, et al. Reduction in memory in passive avoidance learning, exploratory behaviour and synaptic plasticity in mice with a

662 spontaneous deletion in the ubiquitin C-terminal hydrolase L1 gene. Eur J Neurosci. 2008;27: 691–
663 701. doi:10.1111/j.1460-9568.2008.06047.x
664 36. Gong B, Cao Z, Zheng P, Vitolo OV, Liu S, Staniszewski A, et al. Ubiquitin hydrolase Uch-L1 rescues
665 beta-amyloid-induced decreases in synaptic function and contextual memory. Cell. 2006;126:
666 775–788. doi:10.1016/j.cell.2006.06.046
667 37. Liu H, Li W, Rose ME, Hickey RW, Chen J, Uechi GT, et al. The point mutation UCH-L1 C152A
668 protects primary neurons against cyclopentenone prostaglandin-induced cytotoxicity: implications
669 for post-ischemic neuronal injury. Cell Death Dis. 2015;6: e1966. doi:10.1038/cddis.2015.323
670 38. Bheda A, Gullapalli A, Caplow M, Pagano JS, Shackelford J. Ubiquitin editing enzyme UCH L1 and
671 microtubule dynamics: implication in mitosis. Cell Cycle. 2010;9: 980–994.
672 doi:10.4161/cc.9.5.10934
673 39. Pukaß K, Richter-Landsberg C. Inhibition of UCH-L1 in oligodendroglial cells results in microtubule
674 stabilization and prevents α-synuclein aggregate formation by activating the autophagic pathway:
675 implications for multiple system atrophy. Front Cell Neurosci. 2015;9: 163.
676 doi:10.3389/fncel.2015.00163
677 40. Konya C, Hatanaka Y, Fujiwara Y, Uchida K, Nagai Y, Wada K, et al. Parkinson's disease-associated
678 mutations in α-synuclein and UCH-L1 inhibit the unconventional secretion of UCH-L1. Neurochem
679 Int. 2011;59: 251–258. doi:10.1016/j.neuint.2011.05.012
680 41. Liu H, Li W, Ahmad M, Miller TM, Rose ME, Poloyac SM, et al. Modification of ubiquitin-C-terminal
681 hydrolase-L1 by cyclopentenone prostaglandins exacerbates hypoxic injury. Neurobiol Dis.
682 2011;41: 318–328. doi:10.1016/j.nbd.2010.09.020
683 42. Saigoh K, Wang YL, Suh JG, Yamanishi T, Sakai Y, Kiyosawa H, et al. Intragenic deletion in the gene
684 encoding ubiquitin carboxy-terminal hydrolase in gad mice. Nat Genet. 1999;23: 47–51.
685 doi:10.1038/12647
686 43. Sekiguchi S, Kwon J, Yoshida E, Hamasaki H, Ichinose S, Hideshima M, et al. Localization of
687 ubiquitin C-terminal hydrolase L1 in mouse ova and its function in the plasma membrane to block
688 polyspermy. Am J Pathol. 2006;169: 1722–1729. doi:10.2353/ajpath.2006.060301
689 44. Mtango NR, Sutovsky M, Vandevoort CA, Latham KE, Sutovsky P. Essential role of ubiquitin C-
690 terminal hydrolases UCHL1 and UCHL3 in mammalian oocyte maturation. J Cell Physiol. 2012;227:
691 2022–2029. doi:10.1002/jcp.22931
692 45. Gu Y-Q, Chen Q-J, Gu Z, Shi Y, Yao Y-W, Wang J, et al. Ubiquitin carboxyl-terminal hydrolase L1
693 contributes to the oocyte selective elimination in prepubertal mouse ovaries. Sheng Li Xue Bao.
694 2009;61: 175–184.
695 46. Niu W, Spradling AC. Two distinct pathways of pregranulosa cell differentiation support follicle
696 formation in the mouse ovary. Proc Natl Acad Sci USA. 2020;117: 20015–20026.
697 doi:10.1073/pnas.2005570117
698 47. Gray S, Cohen PE. Control of meiotic crossovers: from double-strand break formation to
699 designation. Annu Rev Genet. 2016;50: 175–210. doi:10.1146/annurev-genet-120215-035111
700 48. Zhao H, Chen Z-J, Qin Y, Shi Y, Wang S, Choi Y, et al. Transcription factor FIGLA is mutated in
701 patients with premature ovarian failure. Am J Hum Genet. 2008;82: 1342–1348.
702 doi:10.1016/j.ajhg.2008.04.018
703 49. Soyal SM, Amleh A, Dean J. FIGalpha, a germ cell-specific transcription factor required for ovarian
704 follicle formation. Development. 2000;127: 4645–4654.
705 50. Liang L, Soyal SM, Dean J. FIGalpha, a germ cell specific transcription factor involved in the
706 coordinate expression of the zona pellucida genes. Development. 1997;124: 4939–4947.
707 51. Gura MA, Mikedis MM, Seymour KA, de Rooij DG, Page DC, Freiman RN. Dynamic and regulated
708 TAF gene expression during mouse embryonic germ cell development. PLoS Genet. 2020;16:
709 e1008515. doi:10.1371/journal.pgen.1008515

52. Vourekas A, Zheng K, Fu Q, Maragkakis M, Alexiou P, Ma J, et al. The RNA helicase MOV10L1 binds piRNA precursors to initiate piRNA processing. Genes Dev. 2015;29: 617–629. doi:10.1101/gad.254631.114
53. Aravin AA, van der Heijden GW, Castañeda J, Vagin VV, Hannon GJ, Bortvin A. Cytoplasmic compartmentalization of the fetal piRNA pathway in mice. PLoS Genet. 2009;5: e1000764. doi:10.1371/journal.pgen.1000764
54. Soper SFC, van der Heijden GW, Hardiman TC, Goodheart M, Martin SL, de Boer P, et al. Mouse maelstrom, a component of nuage, is essential for spermatogenesis and transposon repression in meiosis. Dev Cell. 2008;15: 285–297. doi:10.1016/j.devcel.2008.05.015
55. Wang J-J, Ge W, Zhai Q-Y, Liu J-C, Sun X-W, Liu W-X, et al. Single-cell transcriptome landscape of ovarian cells during primordial follicle assembly in mice. PLoS Biol. 2020;18: e3001025. doi:10.1371/journal.pbio.3001025
56. Wang Z, Liu C-Y, Zhao Y, Dean J. FIGLA, LHX8 and SOHLH1 transcription factor networks regulate mouse oocyte growth and differentiation. Nucleic Acids Res. 2020;48: 3525–3541. doi:10.1093/nar/gkaa101
57. Carmell MA, Dokshin GA, Skaletsky H, Hu Y-C, van Wolfswinkel JC, Igarashi KJ, et al. A widely employed germ cell marker is an ancient disordered protein with reproductive functions in diverse eukaryotes. Elife. 2016;5. doi:10.7554/eLife.19993
58. Grive KJ, Hu Y, Shu E, Grimson A, Elemento O, Grenier JK, et al. Dynamic transcriptome profiles within spermatogonial and spermatocyte populations during postnatal testis maturation revealed by single-cell sequencing. PLoS Genet. 2019;15: e1007810. doi:10.1371/journal.pgen.1007810
59. Kedem-Dickman A, Maman E, Yung Y, Yerushalmi GM, Hemi R, Hanochi M, et al. Anti-Müllerian hormone is highly expressed and secreted from cumulus granulosa cells of stimulated preovulatory immature and atretic oocytes. Reprod Biomed Online. 2012;24: 540–546. doi:10.1016/j.rbmo.2012.01.023
60. Walters BJ, Campbell SL, Chen PC, Taylor AP, Schroeder DG, Dobrunz LE, et al. Differential effects of Usp14 and Uch-L1 on the ubiquitin proteasome system and synaptic activity. Mol Cell Neurosci. 2008;39: 539–548. doi:10.1016/j.mcn.2008.07.028
61. Xu Y, Hideshima M, Ishii Y, Yoshikawa Y, Kyuwa S. Ubiquitin C-terminal hydrolase l1 is expressed in mouse pituitary gonadotropes in vivo and gonadotrope cell lines in vitro. Exp Anim. 2014;63: 247–256. doi:10.1538/expanim.63.247
62. Novaira HJ, Yates M, Diaczok D, Kim H, Wolfe A, Radovick S. The gonadotropin-releasing hormone cell-specific element is required for normal puberty and estrous cyclicity. J Neurosci. 2011;31: 3336–3343. doi:10.1523/JNEUROSCI.5419-10.2011
63. Tata B, Huijbregts L, Jacquier S, Csaba Z, Genin E, Meyer V, et al. Haploinsufficiency of Dmxl2, encoding a synaptic protein, causes infertility associated with a loss of GnRH neurons in mouse. PLoS Biol. 2014;12: e1001952. doi:10.1371/journal.pbio.1001952
64. Stamatiades GA, Carroll RS, Kaiser UB. GnRH-A Key Regulator of FSH. Endocrinology. 2019;160: 57–67. doi:10.1210/en.2018-00889
65. Kwon J, Kikuchi T, Setsuie R, Ishii Y, Kyuwa S, Yoshikawa Y. Characterization of the testis in congenitally ubiquitin carboxy-terminal hydrolase-1 (Uch-L1) defective (gad) mice. Exp Anim. 2003;52: 1–9. doi:10.1538/expanim.52.1
66. Kwon J, Mochida K, Wang Y-L, Sekiguchi S, Sankai T, Aoki S, et al. Ubiquitin C-terminal hydrolase L-1 is essential for the early apoptotic wave of germinal cells and for sperm quality control during spermatogenesis. Biol Reprod. 2005;73: 29–35. doi:10.1095/biolreprod.104.037077
67. Alpaugh WF, Voigt AL, Dardari R, Su L, Al Khatib I, Shin W, et al. Loss of Ubiquitin Carboxy-Terminal Hydrolase L1 Impairs Long-Term Differentiation Competence and Metabolic Regulation in Murine Spermatogonial Stem Cells. Cells. 2021;10. doi:10.3390/cells10092265

68. Yuan P, Zhou L, Zhang X, Yao L, Ning J, Han X, et al. UCH-L1 inhibitor LDN-57444 hampers mouse oocyte maturation by regulating oxidative stress and mitochondrial function and reducing ERK1/2 expression. Biosci Rep. 2020;40. doi:10.1042/BSR20201308
69. Stuart T, Butler A, Hoffman P, Hafemeister C, Papalexi E, Mauck WM, et al. Comprehensive Integration of Single-Cell Data. Cell. 2019;177: 1888–1902.e21. doi:10.1016/j.cell.2019.05.031
70. Ajayi AF, Akhigbe RE. Staging of the estrous cycle and induction of estrus in experimental rodents: an update. Fertil Res Pract. 2020;6: 5. doi:10.1186/s40738-020-00074-3
71. Luo C, Zuñiga J, Edison E, Palla S, Dong W, Parker-Thornburg J. Superovulation strategies for 6 commonly used mouse strains. J Am Assoc Lab Anim Sci. 2011;50: 471–478.

FIGURE LEGEND:

Figure 1 – *Clustering of single-cell data and Uchl1 expression*. A) tSNE representation of all cells from the four time point libraries of origin with oocytes denoted in inset. The top 20 most highly expressed oocyte-specific genes are shown to the right of the plot. Log2 fold change above somatic cell expression is denoted by the color bar. B) tSNE plot of *Uchl1* expression in all cells, demonstrating very high expression in a subset of oocytes.

Figure 2 – *UCHL1 protein expression in perinatal mouse ovaries*. Ovaries were collected from mice at E18.5, PND0, PND1, and PND3, paraffin-embedded, sectioned in 5 µm sections, and stained with antibodies against UCHL1 (red) and early oocyte marker TRA98 (green), as well as DAPI (blue). UCHL1 is co-expressed with TRA98 in a subset of oocytes at E18.5, becoming ubiquitously expressed in all oocytes by PND3.

Figure 3 - *UCHL1 protein expression in juvenile and adult mouse ovaries.* Ovaries were collected from mice at PND21, 1 month, 5 months, and 8 months, paraffin-embedded, sectioned in 5 µm sections, and stained with antibody against UCHL1 (red) as well as DAPI (blue). UCHL1 expression persists throughout adult life in oocytes of all follicle stages. Background staining in fibrotic areas is observed in 8-month-old mouse ovaries which are approaching reproductive senescence.

Figure 4 – *UCHL1 knockout mice exhibit severely reduced fertility with fewer litters produced and fewer pups per litter.* A) Cumulative pups resulting from the fertility study were plotted for each genotype (n=3 each wild-type and knockout breeders, n=4 heterozygous breeders). B) Knockout females produce significantly fewer litters than their wild-type counterparts (p=0.0.042) as well as fewer pups per litter (p=0.0002). Knockout also produce significantly fewer pups per litter than their heterozygous counterparts (p=0.008) despite heterozygotes also demonstrating a non-significant trend of subfertility.

Figure 5 – *Hormonal cyclicity and response are significantly affected in knockout females*. A) Mice were assessed for vaginal cytology daily for two weeks starting at 40 days of age, and percentage of time spent in each cycle stage was averaged between animals in a genotype (n=3 for wildtype, n=6 for heterozygotes, and n=5 for knockouts). Knockout animals spend significantly less time in proestrus compared to age-matched wild-type females (p=0.0085) as well as longer in diestrus (p=0.0434). While non-significant, there is a trend for knockout females spending a greater percentage of time in estrus as well. Heterozygous animals also exhibit disrupted cycling, also with significantly less time in proestrus compared to age-matched wild-type females (p=0.0145) as well as longer in diestrus (p=0.0456). B) At 28 days of age, animals of all genotypes (n=13 wild-type, 14 heterozygous, 3 knockout animals) were super-ovulated using standard PMSG and HCG protocols. Retrieved oocytes were collected from each animal, counted, and averaged per genotype. Significantly fewer oocytes were recovered from knockout animals compared to their heterozygous or wild-type counterparts (p=0.050).

Figure 6 – *Follicle abundance and AMH levels are initially similar between all genotypes of mice*. A) Ovaries from female mice at 1 month of age were collected, paraffin-embedded, and stained by standard hematoxylin and eosin protocols (n=8 wild-type, 6 heterozygous, 6 knockout animals). Ovarian follicle counts were quantified using two sections on every fourth slide of sectioned ovary to capture all follicle stages without over-counting of larger follicles. Follicle counts were normalized to the section area to account for size differences between different ovaries. No significant differences were observed in follicle densities for any genotype with the exception of significantly greater density of primordial follicles in heterozygous ovaries compared to wild-type or knockout ovaries (p=0.0308). B) Follicle

abundance is consistent with serum AMH, which are not significantly different among the genotypes at 2.5 months of age. C) Representative image of a 1-month-old wild-type ovary with high magnification inset. D) Representative image of a 1-month-old heterozygous ovary with high magnification inset. E) Representative image of a 1-month-old knockout ovary with high magnification inset. White arrows denote degenerating or atretic follicles.

Figure 7 – *Follicle abundance and ovarian volume is significantly altered in knockout ovaries during mid-reproductive age*. A) Ovaries from female mice at 5 months of age were collected, paraffin-embedded, and stained by standard hematoxylin and eosin protocols (n=4 wild-type, 2 heterozygous, 4 knockout animals). Ovarian follicle counts were quantified using two sections on every fourth slide of sectioned ovary to capture all follicle stages without over-counting of larger follicles. Follicle counts were normalized to the section area to account for size differences between different ovaries. Primordial follicles are significantly enriched in knockout ovaries compared to age-matched wild-type or heterozygous ovaries (p=0.0206 and p=0.0443, respectively), while all other follicle stages show a non-significant increase in density in knockout ovaries B) Commensurate with altered folliculogenesis, 5-month-old knockout ovaries are also significantly smaller than age-matched wild-type or homozygous ovaries when normalized to body size (p=0.050; n=3 wild-type, 5 heterozygous, 5 knockout animals) C) Representative image of whole ovaries obtained from 5-month-old wild-type and knockout animals, demonstrating a visible difference in ovarian volume. D) Representative image of a 5-month-old wild-type ovary with high magnification inset. E) Representative image of a 5-month-old heterozygous ovary with high magnification inset. F) Representative image of a 5-month-old knockout ovary with high magnification inset.

Supplemental Figure 1 – *tSNE plots of oocyte markers in single-cell data*. *Dazl* (A) and *Ddx4* (B) were used to identify the oocyte population within the data set. Log2 fold change above somatic cell expression is denoted by the associated color bar.

Supplemental Figure 2 – *Uchl1 expression is highly correlated with expression of other oocyte regulators at PND0*. PND0 oocyte gene expression was mined from the ovarian single-cell data by Wang et al [55]. Normalized gene expression counts for *Uchl1* compared to *Sohlh1*, *Figla*, and *Lhx8* were plotted in Graphpad Prism and a linear regression applied. Correlation analysis of *Uchl1* with oocyte-specific transcriptional regulators (A) *Figla*, (B) *Sohlh1*, and (C) *Lhx8* revealed significant correlations between the expression of both genes (r=0.7895, r=0.7700, and r=0.7074 respectively), suggesting potential co-regulator of several master regulators of oocyte development at this developmental time.

Supplemental Figure 3 – *UCHL1 knockout animals have no detectable UCHL1 expression in the ovary*. Ovaries from wild-type and knockout animals at 1 and 5 months of age were paraffin-embedded, sectioned in 5 µm sections, and stained with antibody against UCHL1 (red) as well as DAPI (blue). While UCHL1 is detectable in all oocytes of wild-type ovaries, there is no detectable UCHL1 expression, as expected, in any cells of the knockout ovaries.

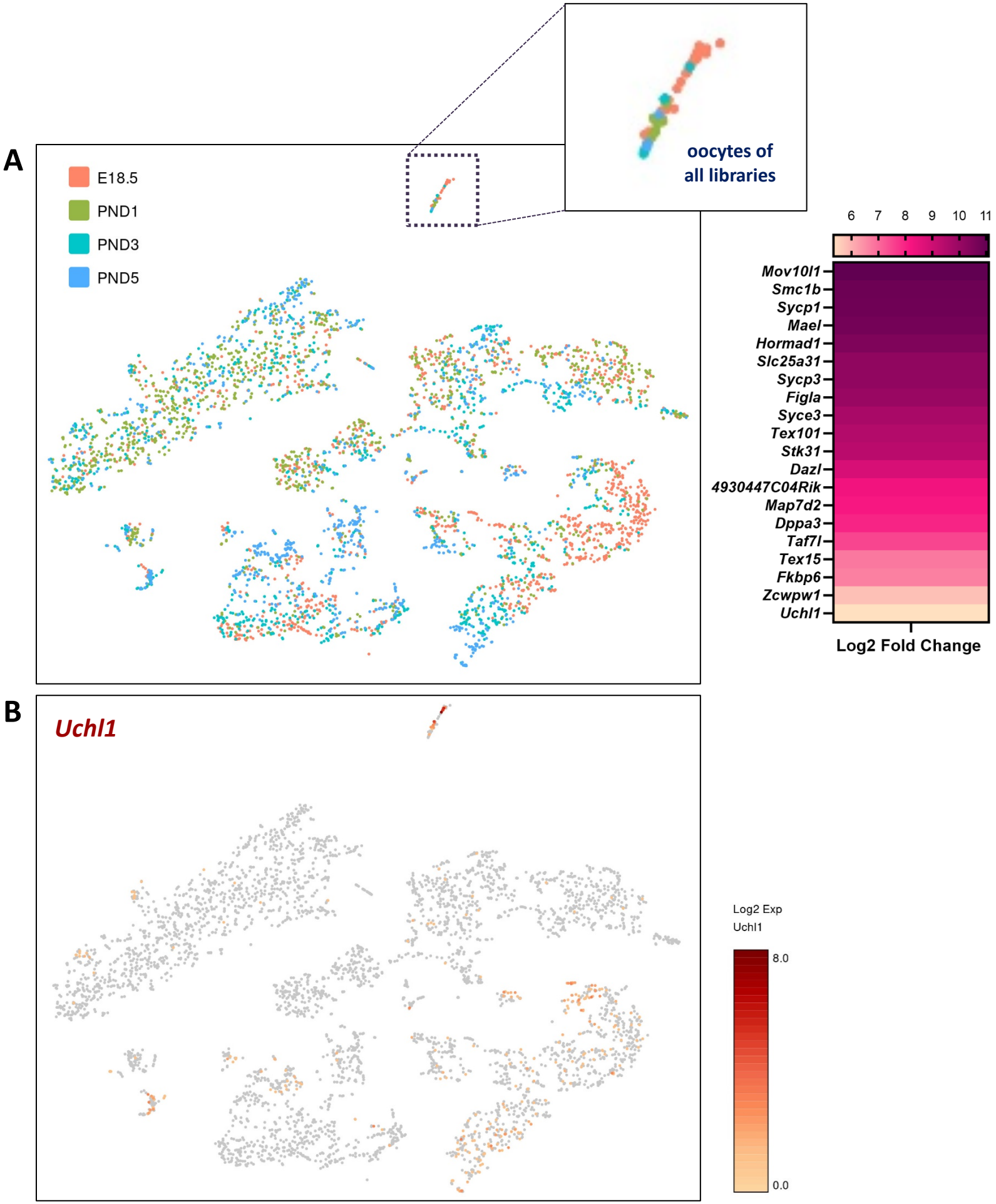
A
E18.5
PND1
PND3
PND5
oocytes of
all libraries
6
7
8
9
10
11
Mov10l1
Smc1b
Sycp1
Mael
Hormad1
Slc25a31
Sycp3
Figla
Syce3
Tex101
Stk31
Dazl
4930447C04Rik
Map7d2
Dppa3
Taf7l
Tex15
Fkbp6
Zcwpw1
Uchl1
Log2 Fold Change
B
Uchl1
Log2 Exp
Uchl1
8.0
0.0

Figure 1

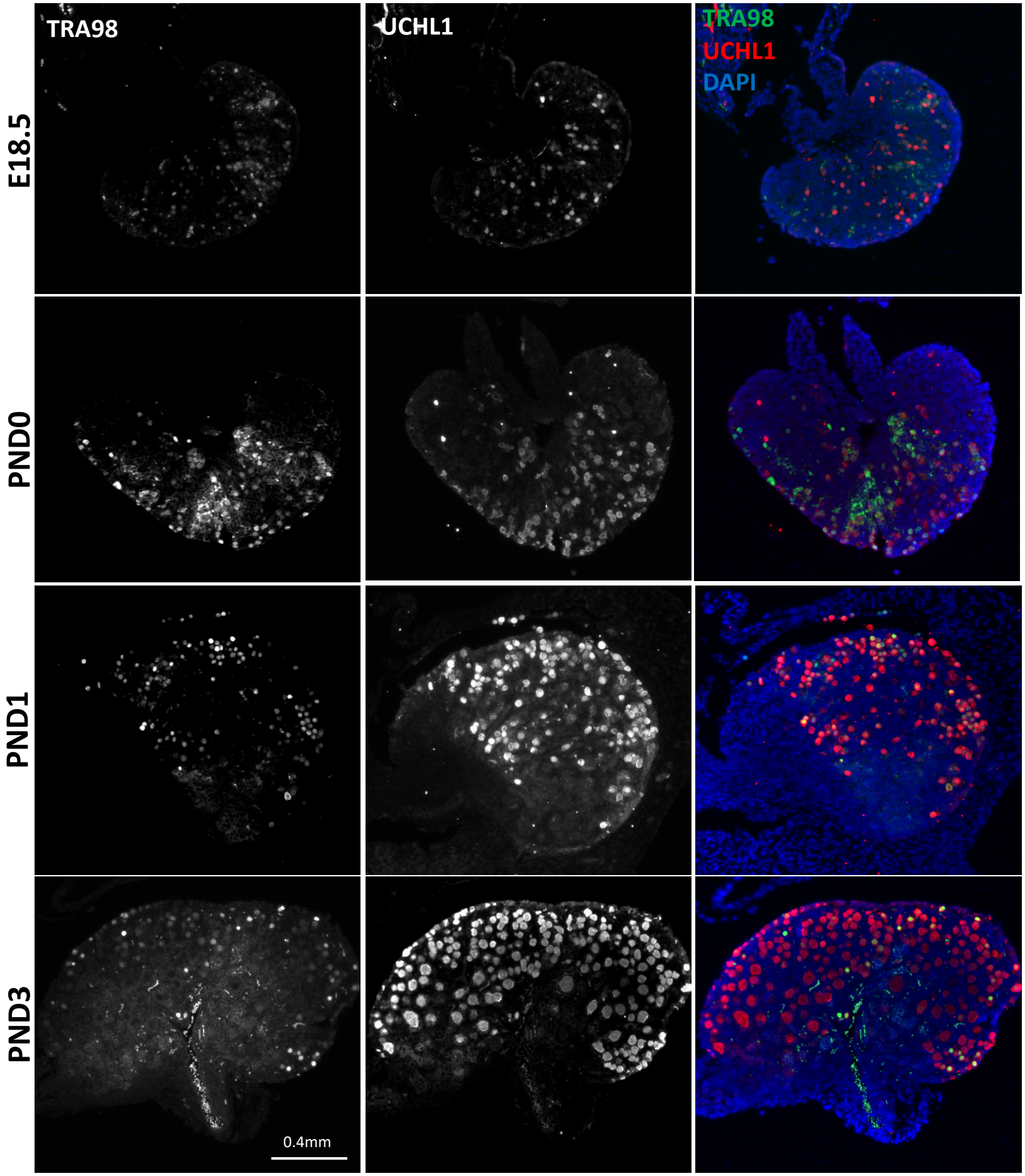

Figure 2

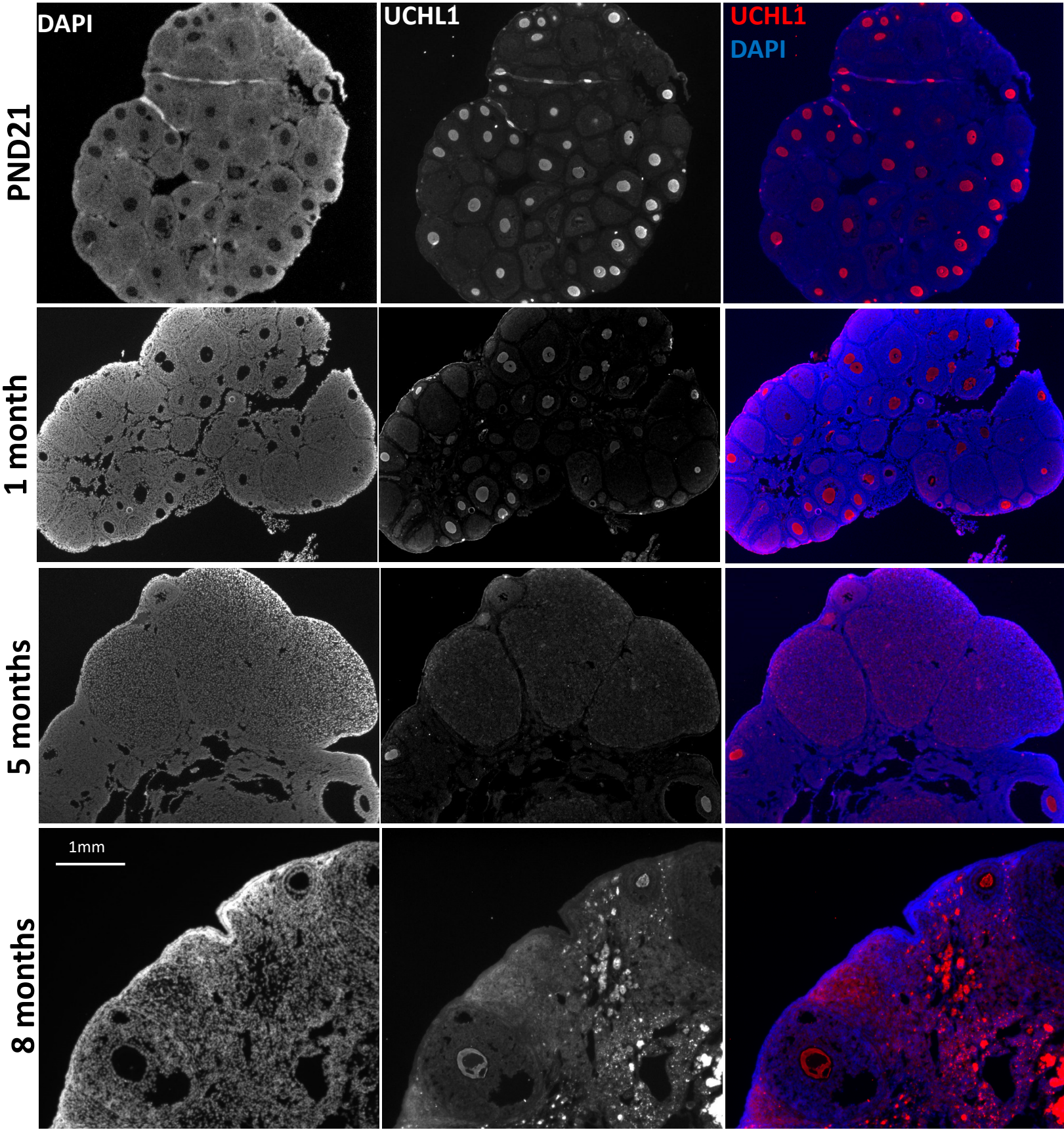

Figure 3

A

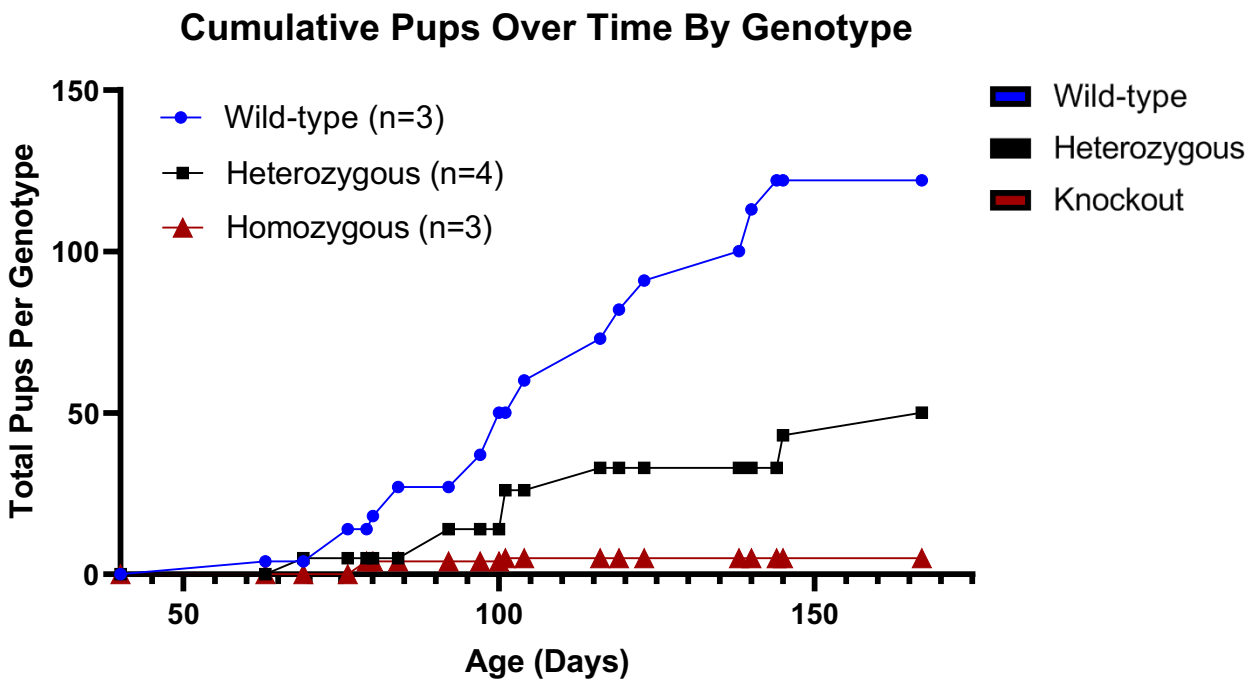
Cumulative Pups Over Time By Genotype
Total Pups Per Genotype
150
100
50
0
50
100
150
Age (Days)
Wild-type (n=3)
Heterozygous (n=4)
Homozygous (n=3)
Wild-type
Heterozygous
Knockout

B

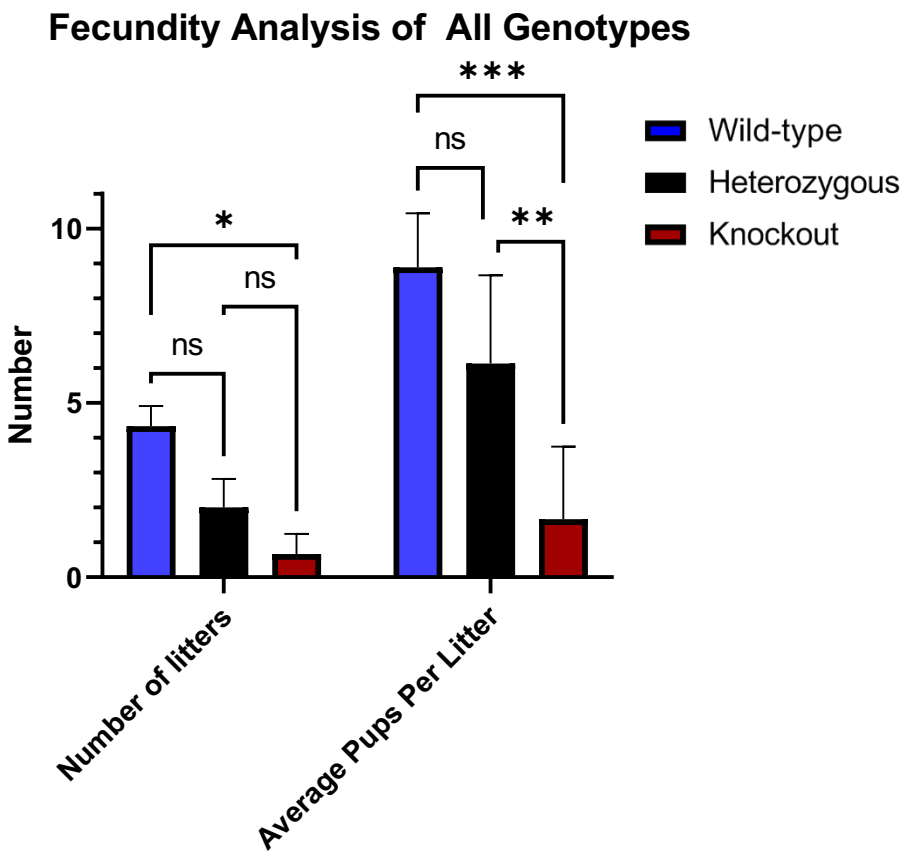
Fecundity Analysis of All Genotypes
Number
10
5
0
*
ns
ns
***
ns
**
Number of litters
Average Pups Per Litter
Wild-type
Heterozygous
Knockout

Figure 4

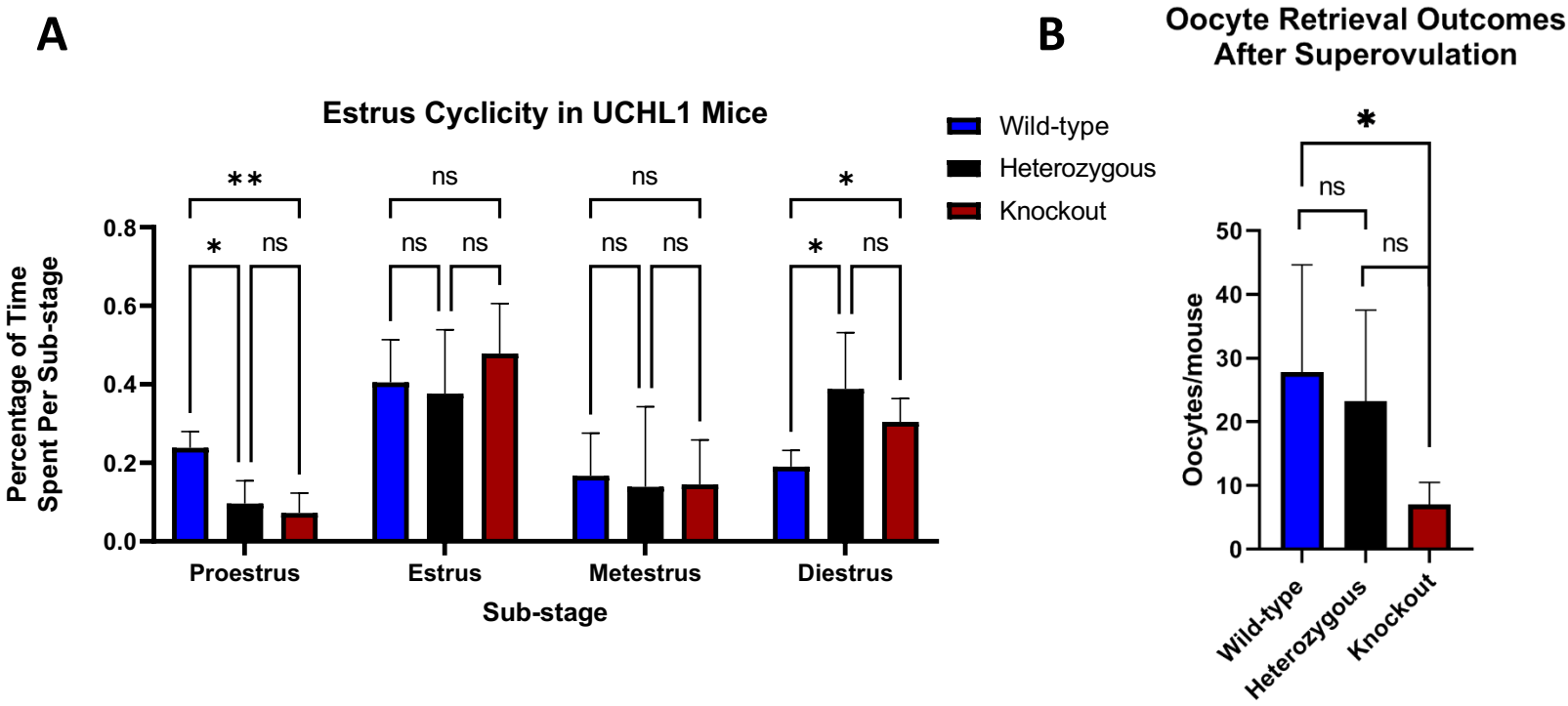
A
Estrus Cyclicity in UCHL1 Mice
Percentage of Time Spent Per Sub-stage
0.0
0.2
0.4
0.6
0.8
**
*
ns
ns
ns
ns
ns
ns
ns
*
*
ns
Proestrus
Estrus
Metestrus
Diestrus
Sub-stage
Wild-type
Heterozygous
Knockout
B
Oocyte Retrieval Outcomes After Superovulation
Oocytes/mouse
0
10
20
30
40
50
*
ns
ns
Wild-type
Heterozygous
Knockout

Figure 5

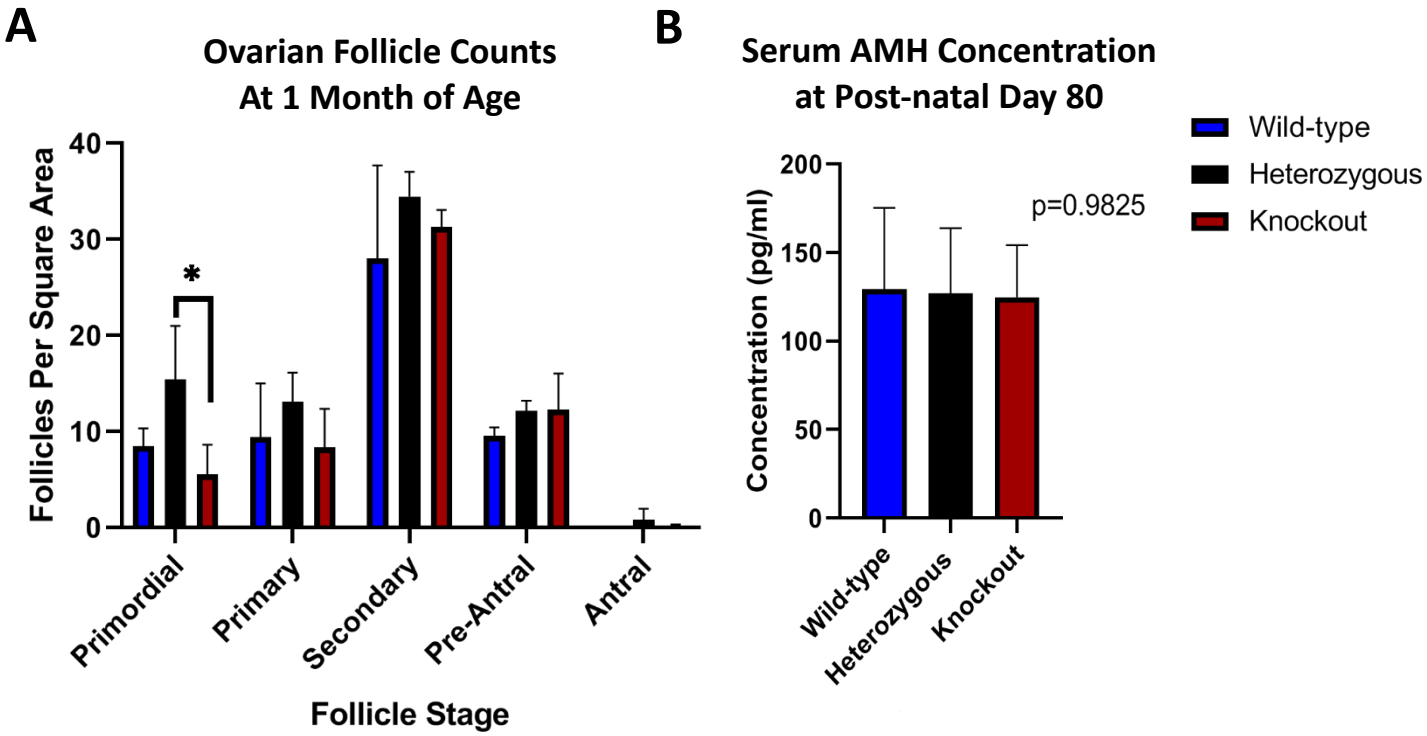
A
Ovarian Follicle Counts
At 1 Month of Age
Follicles Per Square Area
40
30
20
10
0
*
Primordial
Primary
Secondary
Pre-Antral
Antral
Follicle Stage
B
Serum AMH Concentration
at Post-natal Day 80
Concentration (pg/ml)
200
150
100
50
0
p=0.9825
Wild-type
Heterozygous
Knockout
Wild-type
Heterozygous
Knockout

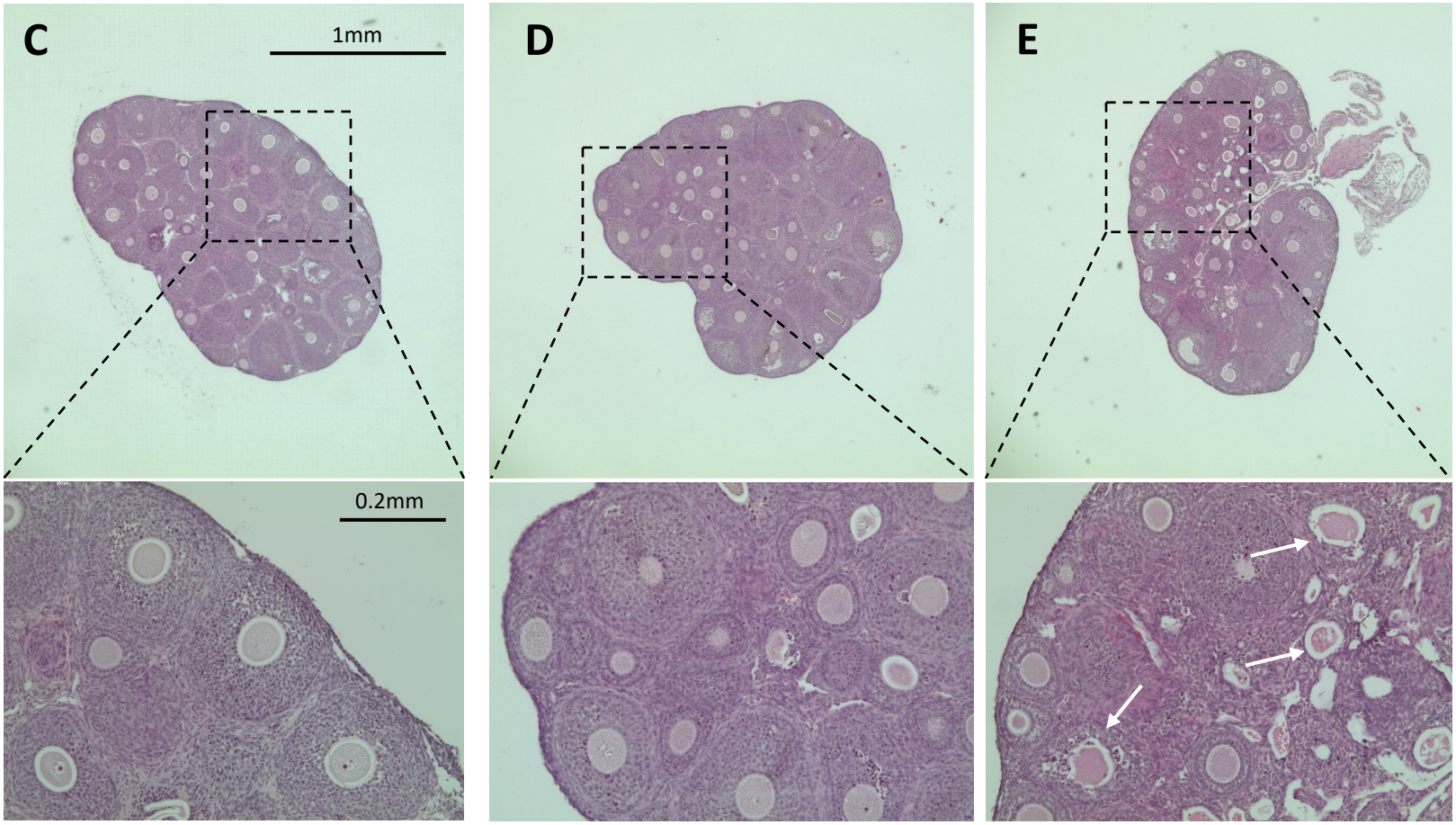
C
1mm
0.2mm
D
E

Figure 6

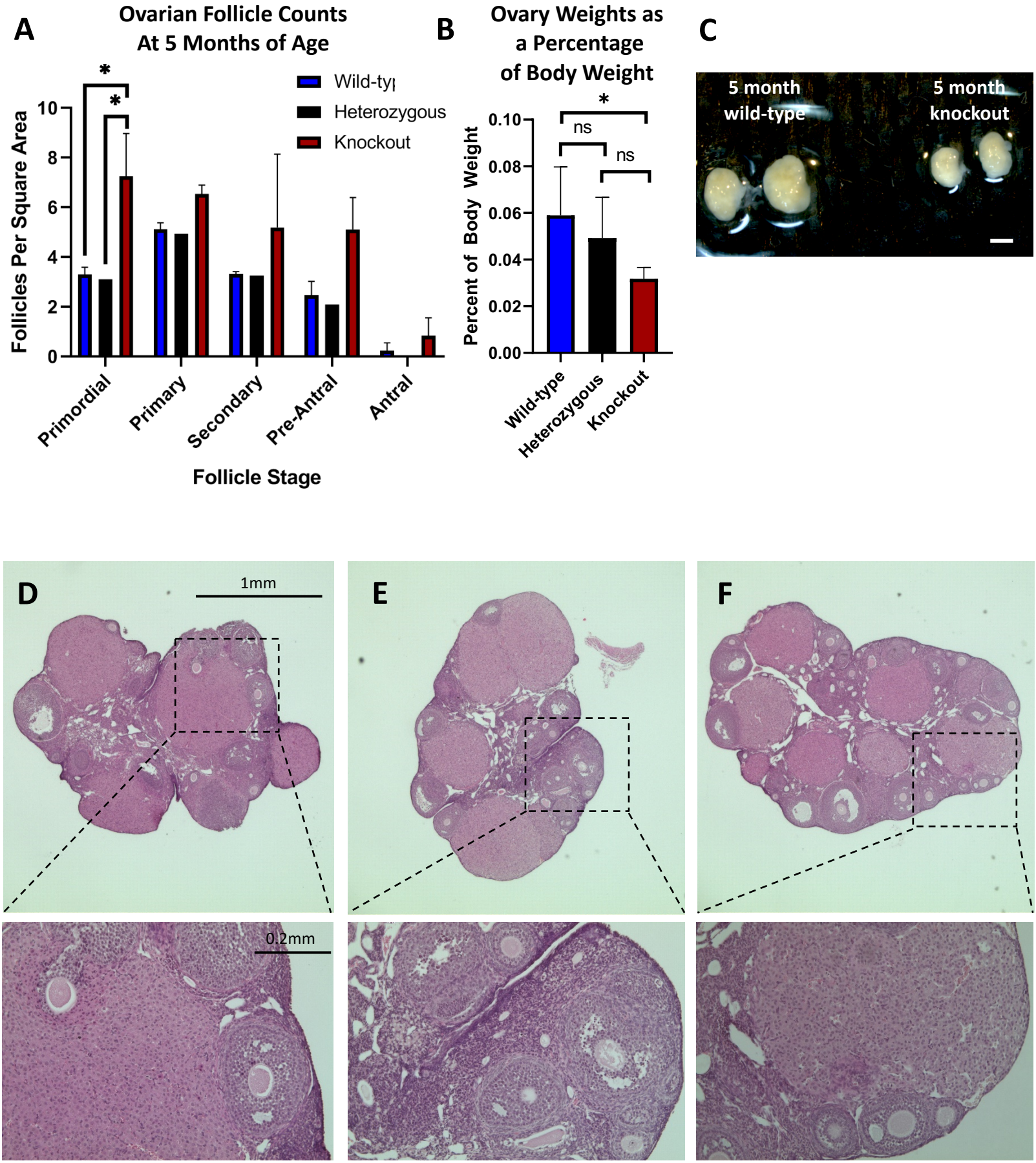
A
Ovarian Follicle Counts
At 5 Months of Age
Wild-type
Heterozygous
Knockout
Follicles Per Square Area
Primordial
Primary
Secondary
Pre-Antral
Antral
Follicle Stage
B
Ovary Weights as
a Percentage
of Body Weight
Percent of Body Weight
ns
ns
Wild-type
Heterozygous
Knockout
C
5 month
wild-type
5 month
knockout
D
1mm
0.2mm
E
F

Figure 7

A

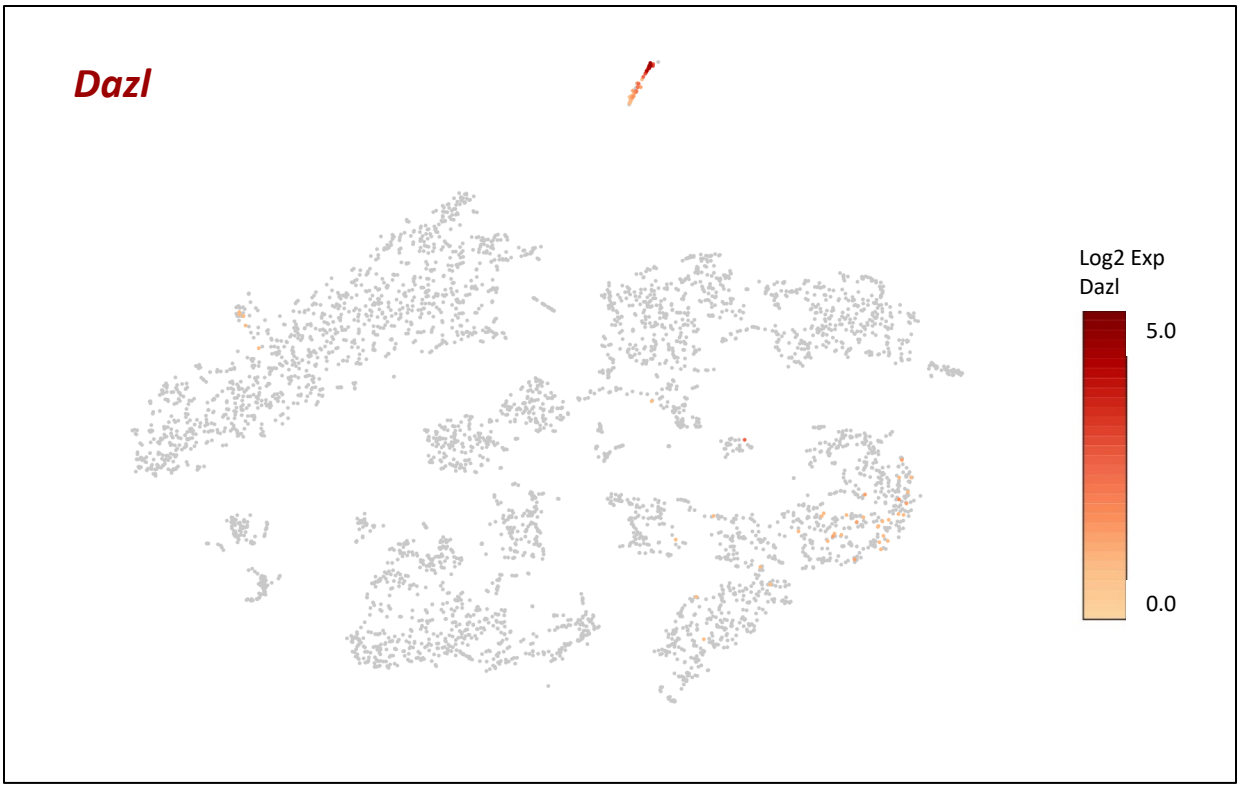

B

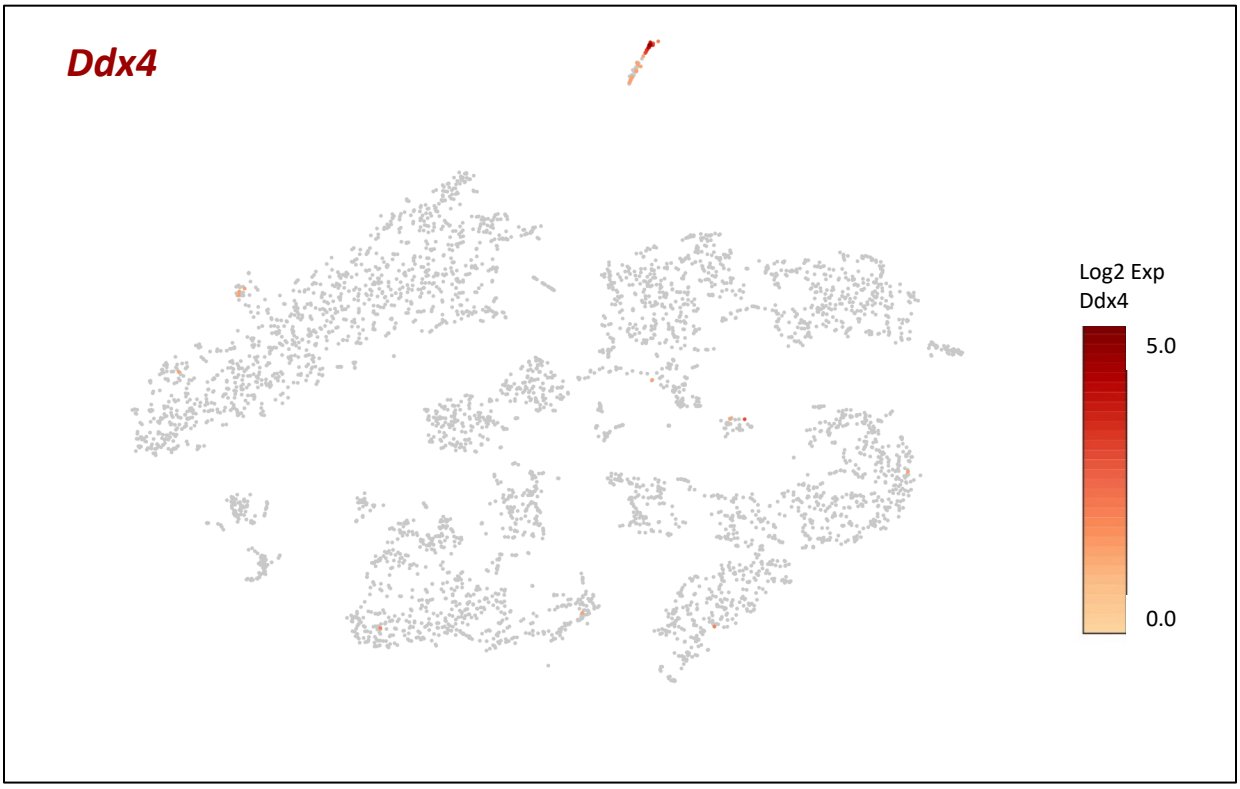

Supp 1

A

Relative Expression Between *Uchl1* and *Figla* Expression in PND0 Oocytes

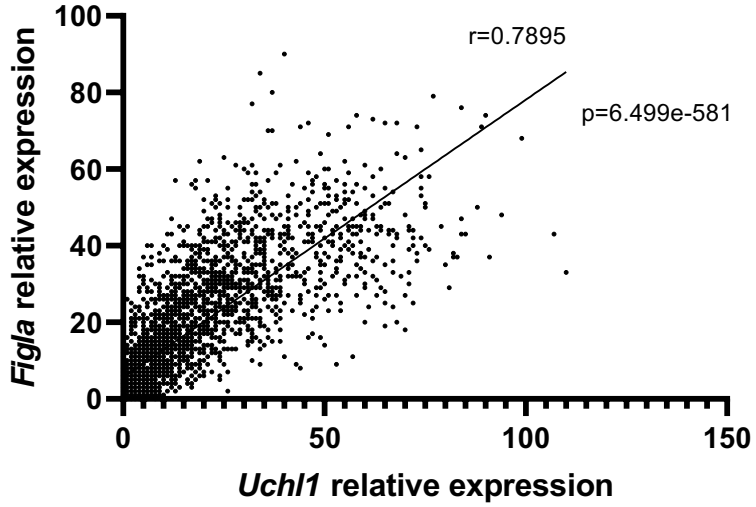

B

Relative Expression Between *Uchl1* and *Sohlh1* Expression in PND0 Oocytes

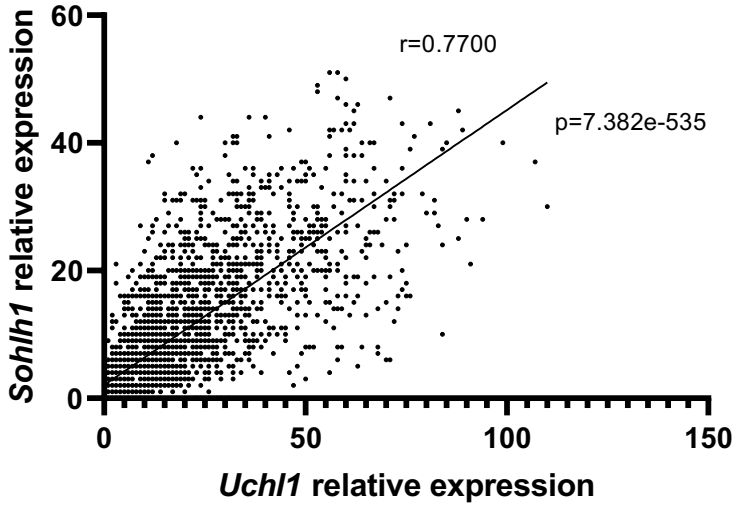

C

Relative Expression Between *Uchl1* and *Lhx8* Expression in PND0 Oocytes

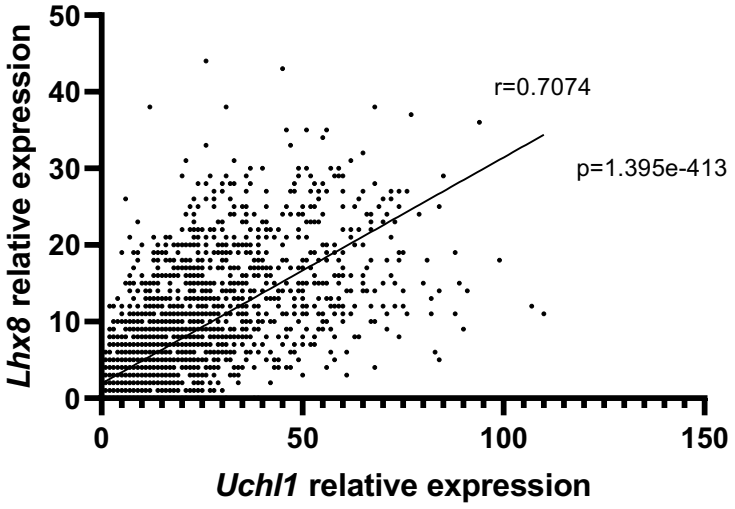

Supp 2

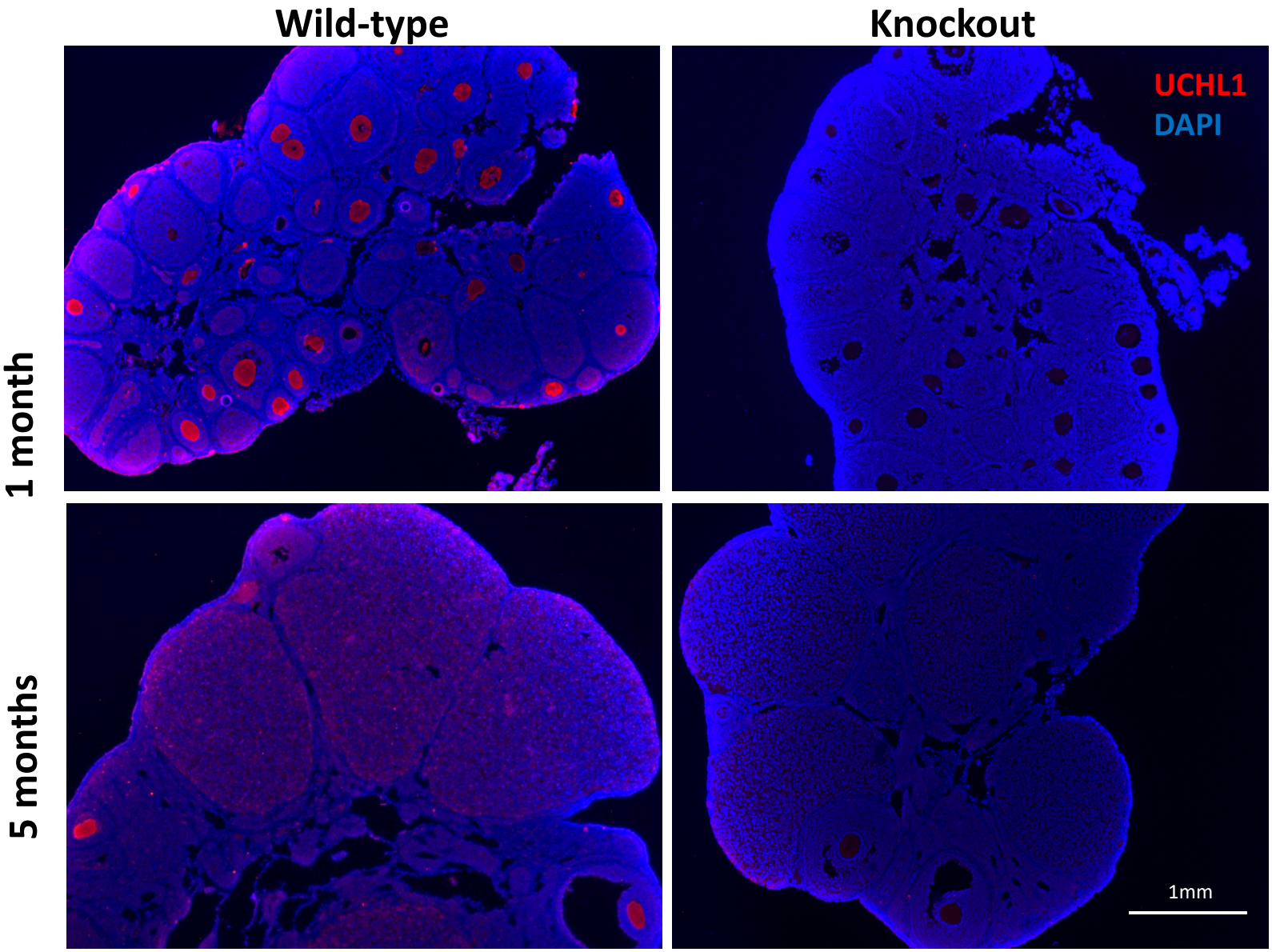

Supp 3